PDAT regulates PE as transient carbon sink alternative to triacylglycerol in Nannochloropsis

Juan Yang, Jin Liu, Yufang Pan, Eric Maréchal, Alberto Amato, Meijing Liu, Yangmin Gong, Yantao Li, Hanhua Hu

PDAT regulates PE as transient carbon sink alternative to triacylglycerol in *Nannochloropsis*.

Juan Yang,[a,f,1] Jin Liu,[b,1] Yufang Pan,[a] Eric Maréchal,[c] Alberto Amato,[c] Meijing Liu,[b] Yangmin Gong,[d] Yantao Li,[e] and Hanhua Hu[a,2]

[a] Key Laboratory of Algal Biology, Institute of Hydrobiology, Chinese Academy of Sciences, Wuhan 430072, China

[b] Laboratory for Algae Biotechnology and Innovation, College of Engineering, Peking University, Beijing100871, China

[c] Laboratoire de Physiologie Cellulaire Végétale, Université Grenoble Alpes, CEA, CNRS, INRA, IRIG-LPCV, 38054 Grenoble Cedex 9, France

[d] Key Laboratory of Biology and Genetic Improvement of Oil Crops, Ministry of Agriculture, Oil Crops Research Institute of Chinese Academy of Agricultural Sciences, Wuhan 430062, China

[e] Institute of Marine and Environmental Technology, University of Maryland Center for Environmental Science and University of Maryland Baltimore County, Baltimore, Maryland 21202, USA

[f] University of Chinese Academy of Sciences, Beijing 100049, China

Short title: PDAT-mediated massive turnover of PG and PE for TAG synthesis

Number of printed pages: ??

[1] These authors contributed equally to this work.
[2] Address correspondence to hanhuahu@ihb.ac.cn.
The author responsible for distribution of materials integral to the findings presented in this article in accordance with the policy described in the Instructions for Authors (www.plantcell.org) is: Hanhua Hu (hanhuahu@ihb.ac.cn).

ABSTRACT (~200 words)

Nannochloropsis oceanica is equipped with more than ten diacylglycerol:acyltransferases (NoDGATs) involved in triacylglycerol (TAG) production, pointing to the puzzling role of the unique phospholipid:diacylglycerol acyltransferase (NoPDAT) it also contains. NoPDAT expression could complement a TAG-deficient yeast phenotype and use a broad range of acyl-donors *in vitro*. Overexpression and knockdown experiments demonstrated the role of *NoPDAT* in modulating the transfer of palmitoyl (16:0) and palmitoleyl (16:1) at the *sn*-3 position of diacylglycerol (DAG), contributing a third of TAG accumulation at the onset of stationary growth phase. No compensatory mechanisms via DGAT pathways could be evidenced, showing that the PDAT pathway is a parallel and independent oil-producing route in *N. oceanica.* Subcellular localization analysis suggests that NoPDAT resides at the outermost plastid membrane. Besides phosphatidylglycerol (PG) highlighted in enzymatic assays, *NoPDAT* knockdown led to a two-fold increase in phosphatidylethanolamine (PE), which is attributed to molecular species enriched in 16:0 and 16:1 at the *sn*-2 position, and suggests the critical role of NoPDAT in the turnover of PE and PG specific molecular species for TAG biosynthesis. Interestingly, accumulation of this specific PE was not only triggered by PDAT lesion but also positively correlated with CO_2 availability in the culture, indicating that the specific PE also serves as alternative carbon sink in *N. oceanica.*

Keywords: Chloroplast endoplasmic reticulum, *Nannochloropsis oceanica*, Phosphatidylethanolamine, Phospholipid:diacylglycerol acyltransferase, Triacylglycerol, Turnover, Carbon sink

INTRODUCTION

Eustigmatophytes of the *Nannochloropsis* genus and their close *Microchloropsis* counterparts are oleaginous microalgae, accumulating the neutral lipid triacylglycerol (TAG), and considered as a promising feedstock for a variety of applications, including alga-based biofuels (Vieler et al., 2012b). The *de novo* synthesis of fatty acids (FA) in *Nannochloropsis* species generates myristic, palmitic and palmitoleic acids (14:0, 16:0 and 16:1, respectively) within the plastid, which are exported to the cytosol, where they are converted into acyl-CoAs. In the cytosol, 16:0-CoA is elongated into 18:0-CoA (Dolch et al., 2017) prior to a series of desaturations into 18:1 to18:3, elongation into 20:3, and desaturations that ultimately lead to the formation of eicosapentaenoic acid (20:5). In *Nannochloropsis oceanica* TAG mostly contains 16:0, 16:1, 18:1 and 14:0 (Nobusawa et al., 2017).

Generally, two distinct routes, (i) anacyl-CoA dependent Kennedy pathway and (ii) an acyl-CoA independent pathway, contribute to TAG biosynthesis in many organisms including yeast, land plants, and algae (Sorger and Daum, 2003; Chapman and Ohlrogge, 2012; Xu et al., 2018). On the one hand, the Kennedy pathway starts with glycerol-3-phosphate and involves a set of acyltransferases that pull the acyl moiety from acyl-CoAs to the glycerol backbone. *N. oceanica* contains a single glycerol-3-phosphate acyltransferase (GPAT) transferring acyls to the *sn*-1 position (Nobusawa et al., 2017). Then four lysophosphatidic acid acyltransferases (LPAT) add a second acyl at the *sn*-2 position, using acyl-CoA donors. The function of NoLPAT1, NoLPAT2, NoLPAT3 and NoLPAT4 has been unraveled by the analysis of single- and multiple-gene knockouts (Nobusawa et al., 2017). NoLPAT1 is mainly involved in the transfer of 16:1 to the *sn*-2 position of precursors used for phosphatidylcholine (PC) and the betaine lipid (diacylglycerol-N,N,N-trimethylhomoserine, DGTS) biosynthesis. This isoform is not involved into TAG biosynthesis. By contrast, NoLPAT4 transfers 16:0 to the *sn*-2 position

of a pool of phosphatidic acid strictly dedicated to TAG production. NoLPAT2 and NoLPAT3 are involved in both membrane lipid and TAG production. Genetic studies support some functional overlap among NoLPAT1, NoLAPT2 and NoLPAT3 in membrane lipids, but the *lpat2;3* double KO produced substantially less phosphatidylethanolamine (PE). In brief, NoLPAT2 and NoLPAT3 are mainly involved in the transfer of 18:1 at the *sn*-2 position of precursors used for PC, PE and that of 16:0 at the *sn*-2 position of precursors for TAG (Nobusawa et al., 2017). Eventually, diacylglycerol (DAG) acyltransferase (DGAT) catalyzes the last and committing step for TAG biosynthesis (Chapman and Ohlrogge, 2012). Many microalgae harbor a high copy number of DGAT-encoding genes, e.g., more than 10 copies in *N. oceanica* (Vieler et al., 2012b; Li et al., 2014b). By contrast, land plants typically maintain no more than two copies, e.g., one type I (DGAT1) and one type II (DGAT2) in Arabidopsis (Xu et al., 2018). Functional characterization of algal DGATs have demonstrated their overlapping yet complementary roles in the spatial and temporal control of TAG biosynthesis with diverse patterns of molecular species (Liu et al., 2016a; Wei et al., 2017a; Xin et al., 2017; Zienkiewicz et al., 2017; Mao et al., 2019). Manipulation of *DGAT* genes via rational engineering has therefore a potential to not only increase TAG level but also tailor FA composition for particular uses (Liu et al., 2016a; Xin et al., 2017).

On the other hand, the acyl-CoA independent pathway for TAG biosynthesis is mediated by phospholipid:diacylglycerol acyltransferase (PDAT), transferring an acyl moiety from the *sn*-2 position of a membrane glycerolipid, usually a phospholipid, to the *sn*-3 position of DAG (Dahlqvist et al., 2000). In the yeast *Saccharomyces cerevisiae*, knockout and overexpression of the PDAT-encoding gene *LRO1* supported its indispensable contribution to TAG biosynthesis (Oelkers et al., 2000), together with the type II DGAT-encoding gene *DGA1* (Oelkers et al., 2002; Sandager et al., 2002).Yet the relative contributions of PDAT and DGA1 are growth stage-dependent: PDAT contributes

more at the exponential growth stage while DGA1 contributes more at the stationary stage (Oelkers et al., 2002). Albeit showing activities on a broad range of polar lipids, *S. cerevisiae* PDAT prefers the zwitterionic phospholipids PE and PC, particularly the former, as acyl donor for TAG biosynthesis (Dahlqvist et al., 2000; Ghosal et al., 2007; Feng et al., 2019). In contrast to the presence of a single copy of *PDAT* gene in yeast and algae, many land plants experienced gene expansion events during evolution and contain multiple *PDAT* copies (Pan et al., 2015; Falarz et al., 2020). Unlike in *S. cerevisiae*, neither overexpression nor knockout of *PDAT1* in Arabidopsis affected the seed lipid profiles (Ståhl et al., 2004; Mhaske et al., 2005). Nevertheless, in a *dgat1* null mutant of Arabidopsis, knockdown of *PDAT1* leads to a more severe decrease in seed TAG level, suggesting that *PDAT1* and *DGAT1* have overlapping activities at least in seeds (Zhang et al., 2009). By contrast, in actively growing tissues such as developing leaves, *PDAT1* functions independently and contributes more than *DGAT1* to TAG biosynthesis, by diverting FA from membrane lipids (Fan et al., 2013a, 2013b). Arabidopsis PDAT1 has a similar substrate specificity as that of *S. cerevisiae* PDAT, using PE and PC as acyl donors, as evidenced by the increase in PE and PC in a *pdat1* mutant and decrease in PE and PC in a *PDAT1*-overexpressing line (Fan et al., 2013a, 2013b).

While well documented in yeast and land plants, PDAT from algae was less scrutinized. Most detailed biochemical and physiological characterization are restricted to green algae, especially *Chlamydomonas reinhardtii* (Yoon et al., 2012; Liu et al., 2016b). Differing from yeast or Arabidopsis enzymes, *C. reinhardtii* PDAT can use a broad range of substrates including phospholipids, glycolipids and DAG as acyl donors. Still, *in vitro* enzymatic assays highlighted an apparent preference of *C. reinhardii* PDAT for anionic phospholipids such as phosphatidylinositol (PI), phosphatidylserine (PS) and phosphatidylglycerol (PG) (Yoon et al., 2012). Intriguingly, it is believed that *C. reinhardtii* PDAT resides in the chloroplast, although the precise localization remains to

be experimentally confirmed, and mediates turnover of chloroplast membrane lipids for TAG biosynthesis particularly under non-stress (favorable growth) conditions (Yoon et al., 2012). By contrast, the three type II *DGAT* genes in *C. reinhardtii*, *CrDGTT1*, *CrDGTT2* and *CrDGTT3,* are predominantly active under stress conditions rather than favorable growth conditions (Liu et al., 2016a).

Altogether, the roles of PDAT and DGAT seem evolutionarily conserved, namely, PDAT mediating membrane lipid turnover and functioning under favorable growth conditions, such as in *S. cerevisiae* and *C. reinhardtii* or developing leaves of Arabidopsis, while DGAT function is apparently predominant following growth arrest. The context in which PDAT might operate, *i.e.* in close relation with the ER or the plastid, is unknown in such clades as Stramenopiles/Heterokonts, whose cells contain plastids originating from a secondary endosymbiosis, bounded by four membranes, with the outermost being related to the endomembrane system. This outermost membrane is known as the chloroplast endoplasmic reticulum (cER) or epiplastid membrane, and its lipid composition has not yet been determined (Petroutsos et al., 2014; Flori et al., 2016; Dolch et al., 2017).

Unlike *C. reinhardtii*, the stramenopile alga *N. oceanica* has been recognized as an industrially important single-cell factory for lipid production because of its fast growth and high lipid content (Ma et al., 2016). Genome data (Vieler et al., 2012b; Wang et al., 2014) and a variety of forward and reverse genetic tools (Wang et al., 2016; Wei et al., 2017b; Poliner et al., 2018a, 2018b, 2020) are available, providing solid foundation to study lipogenesis. *N. oceanica* harbors thirteen *DGAT* genes (two type I referred to as *NoDGAT1A* and *NoDGAT1B*, and eleven type II referred to as *NoDGAT2A* through *NoDGAT2K*) (Li et al., 2014b) versus six in *C. reinhardtii* (one type I and five type II) (Boyle et al., 2012). Although both type I and type II *N. oceanica* DGATs show activities for TAG biosynthesis *in vitro*, their roles *in vivo* depend on growth conditions:

NoDGAT1A, NoDGAT2A, and NoDGAT2D operate under stress conditions, whereas NoDGAT2C, NoDGAT2J and NoDGAT2K operate more under non-stress conditions (Wei et al., 2017a; Xin et al., 2017, 2019). The differences in the number of functional DGATs between *N. oceanica* and *C. reinhardtii* and the presence of DGATs that contribute to non-stress associated TAG biosynthesis in *N. oceanica* raise the questions whether *N. oceanica* PDAT is critical, and under what conditions and to what extent it contributes to TAG biosynthesis.

In the present study, we addressed the function of NoPDAT in *N. oceanica*. NoPDAT resides at the cER, where both plastid and ER lipids are presumed to be present. *In vitro* assays supported that NoPDAT could use a broad range of glycolipids and phospholipids and suggested an apparent preference for PG as acyl donor. Genetic analysis showed that *NoPDAT* contributed at least 30% to TAG biosynthesis under nitrogen limited conditions and seemed determinant in the relative proportion of 16:0 and 16:1 at position *sn*-3 of TAG. In the cellular context, the knockdown of *NoPDAT* caused an increase, regulated by CO_2 availability, of PE with 16:0, 16:1 or 18:1 and of PG with 16:0 and 16:1, at position *sn*-2 of the lipid glycerol backbone. Our study highlights the role of NoPDAT in mobilizing membrane lipids, particularly PE and PG, in the massive biosynthesis of TAG in *N. oceanica* and suggests that the saturated/monounsaturated acyl PE can serve as a potential lipid sink under stress with high CO_2 level.

RESULTS

Cloning and Bioinformatics Analysis of the *PDAT* Gene from *N. oceanica*

The sequenced genome of *N. oceanica* contains a single PDAT-encoding gene candidate (Vieler et al., 2012b; Wang et al., 2014). We obtained the corresponding full-length cDNA (referred to as *NoPDAT*), which consists of a 136-bp 5' untranslated region, a 242-bp 3' untranslated region, and a 2,835-bp coding sequence interrupted by four introns.

Analysis of the polypeptide sequence of NoPDAT against the conserved domain database of the National Center for Biotechnology Information (NCBI) indicated that this protein belongs to the membrane-bound *O*-acyltransferase family and contains a phosphatidylcholine-sterol *O*-acyltransferase domain spanning from 251 to 944 amino acid residues. Transmembrane helix prediction with the TMHMM method (Krogh et al., 2001) suggested the presence of a transmembrane domain (spanning 186-205 amino acid residues) at the N-terminus of NoPDAT (Supplemental Figure 1).

To gain insights into the evolutionary relationship between NoPDAT and other homologs from different phyla, we carried out both a Maximum Likelihood (ML) and a Bayesian phylogenetic inference with a 30-sequence dataset containing six stramenopiles, three basidiomycetes and three ascomycetes, five green algae, one streptophyte and nine sequences from monocots and dicots. Although red algae were supposed to lack PDAT (Lee et al., 2017; Mori et al., 2016), we identified and included in the phylogeny one sequence from *Porphyra umbilicalis*, and two from *Porphyridium purpureum*. Based on preliminary phylogenetic inferences (see Methods for details), red algal PDATs were used as outgroup to root the tree. Bayesian and ML tree topologies were in perfect accordance on the end branches with higher plants PDAT1 (ML support 100, Bayesian posterior probability 1) and PDAT2 (98, 1), fungi (100, 1), and green algae (60, 0.98) clustering accordingly together in robust individual clades. Interestingly, the *Klebsormidium nitens* putative PDAT sequence clustered in both inferences in a basal position to the higher plants (100, 1), in accordance with Streptophyta's evolutionary history (Hori et al., 2014; Wang et al., 2020). Surprisingly, stramenopile PDAT sequences did not cluster together, namely, *N. oceanica* and *Microchloropsis gaditana* (formerly known as *Nannochloropsis gaditana* (Fawley et al., 2015) grouped in a sister clade to *Phytophtora infestans/Plasmoparahalstedii* clade with a weak support (37, 0.74); for diatoms ML did not resolve supraspecific level, while Bayesian analysis robustly (posterior probability=

0.99) clustered diatoms in basal position to the clade grouping plants, fungi, and the other stramenopiles. The polyphyly of stramenopile PDATs may reveal different evolutionary history in diatoms vs eustigmatophyte/oomycetes (Figure 1).

Protein sequence alignment suggested that NoPDAT harbors domains conserved in PDAT polypeptides (Supplemental Figure 1). The analysis of the N-terminal part of NoPDAT using SignalP (Nielsen et al., 2019) did not show any predicted signal peptide. The use of HECTAR, a method to predict subcellular targeting in Heterokonts/Stramenopiles (Gschloessl et al., 2008), together with other prediction tools such as TargetP and ChloroP (Armenteros et al., 2019) or Mitoprot (Claros and Vincens, 1996) did not support any localization in chloroplast or mitochondrion. The absence of any targeting sequence to chloroplast appears consistent with NoPDAT sequence grouping also with non-photosynthetic Stramenopile sequences such as PDAT from oomycota.

Functional Complementation of *NoPDAT* in the TAG-Deficient Yeast and *in vitro* Assay

To evaluate the function of NoPDAT, the coding sequence was introduced into the TAG-deficient yeast strain H1246 (Sandager et al, 2002) for complementation assay. The H1246 strains expressing the empty vector (EV) and *CrDGTT3*, a type II DGAT from *C. reinhardtii* (Liu et al., 2016a), were used as negative and positive controls, respectively. H1246 cells carrying EV gave no detectable level of TAG. By contrast, the expression of *NoPDAT*, similar to *CrDGTT3*, restored TAG biosynthesis in H1246 cells, as indicated by the prominent TAG spot resolved by thin-layer chromatography (TLC) (Figure 2A) and green fluorescence following Bodipy 493/503 staining (a specific dye of neutral lipids) (Figure 2B). These results suggested that NoPDAT is functional in transferring acyl moiety from polar lipids to DAG for TAG assembly. They also emphasize that yeast

subcellular membranes contain substrates that NoPDAT can possibly utilize.

We developed a non-radiolabeled *in vitro* assay for acyltransferases using the microsomal protein fraction from yeast cells as a source of crude enzyme (Liu et al., 2017), following the method described in previous studies to measure the activity and substrate specificity of algal DGATs (Liu et al., 2016a; Wei et al., 2017a; Xin et al., 2017; Mao et al., 2019). A total of ten polar lipids were examined, including phosphate-free glycolipids, *i.e.* monogalactosyldiacylglycerol, MGDG (enriched in 18:3/16:3); digalactosyldiacylglycerol, DGDG (enriched in 18:3/18:3); sulfoquinovosyldiacylglycerol, SQDG (enriched in 18:3/16:0); DGTS (16:1/16:1) and phospholipids, *i.e.* PC (16:1/18:1); PS (16:1/18:1); phosphatidic acid, PA (16:1/18:1); PE (16:1/18:1); PI (enriched in 18:2/16:0) and PG (racemic mix of 16:1/18:1 and 18:1/16:1). Among the tested polar lipids, PG led to the highest activity for TAG formation, while others showed either a low (SQDG, MGDG, and DGDG), very low or no apparent activity (Figure 2C). This *in vitro* analysis confirms that NoPDAT is a glycerolipid acyl transferase, which may accept other substrates than phospholipids, *e.g.* phosphate-free glycolipids. This enzymatic ability to accept multiple membrane glycerolipids as acyl donors is reminiscent to previous observations made with homologs from *C. reinhardtii* and *S. cerevisiae* (Yoon et al., 2012; Feng et al., 2019). Like for the *C. reinhardtii* enzyme, NoPDAT shows a high *in vitro* activity with the anionic lipid PG. However, the *C. reinhardtii* PDAT could also operate on zwitterionic PE or PC substrates *in vitro*. It must be noted that in *N. oceanica*, the native plastid PG molecular species are different from that used in this *in vitro* assay, mainly containing 16:0/16:1, 20:5/16:0 and 20:5/16:1, with a portion of 16:1 being 16:1t a peculiar hexadecenoic acid with a *trans*-desaturation at position Δ3, distinct from palmitoleic acid with a *cis*-desaturation at position Δ9. The apparent differences observed in NoPDAT activity with the substrates tested in the *in vitro* assay, and the apparent lack of activity on zwitterionic

phospholipids, highlight one of the limits of this enzymatic measurement. Indeed, a lack of *in vitro* activity might be attributed either to an intrinsic absence of affinity for the considered substrate, a poor availability of the substrate in the microsomal suspension, non-optimal reaction conditions, or a combination of all these hypotheses.

We also tested the preference of NoPDAT for the structure of the DAG acceptor, including seven 1,2-DAG molecular species and one 1,3-DAG, using PG as the acyl donor (Figure 2D). Based on this assay, NoPDAT could operate on a broad spectrum of DAG acceptors, even belonging to the 1,3 series, with a higher apparent activity with 18:1/18:1, 16:0/18:1 and 18:1/16:0. We did not evaluate the main DAG donor from *N. oceanica*, 16:1/16:0 (Nobusawa et al., 2017), which was not commercially available.

Altogether, this *in vitro* assay validates the molecular activity of the *N. oceanica* enzyme as a canonical PDAT, with the potential to use various membrane glycerolipids as acyl donors and various DAG species as acyl acceptors. It must be noted that, due to the constrains of available membrane lipid and DAG substrates, the molecular species used in this *in vitro* assay differed from the acyl profiles of each lipid class encountered naturally in *N. oceanica*. The actual substrates used by NoPDAT requires therefore, like for previous studies performed in other organisms, complementary genetic analyses.

Subcellular Localization of NoPDAT at the cER

PDAT proteins are membrane-bound and usually reside at the endoplasmic reticulum (ER) in higher plants and yeast (Dahlqvist et al., 2000; Kim et al., 2011). By contrast, the compartmentalization for green algal PDAT remains ambiguous and lacks experimental evidence (Yoon et al., 2012; Liu et al., 2016b). It is worth noticing that in Heterokonts/Stramenopilesthe plastid evolved from a secondary endosymbiosis and is bounded by four membranes (Fussy and Obornik, 2018); the outermost membrane, referred to as cER, is related to the ER and directly connected with the outer membrane

of the nuclear envelope (Gibbs, 1979; Flori et al., 2016).

To get insight on the localization of NoPDAT, we fused the *NoPDAT* coding sequence with the enhanced green fluorescent protein (eGFP) upstream and introduced it into *N. oceanica* for live cell observation. The eGFP alone was used as control. Laser confocal scanning microscopy analyses showed that in the control transformants the eGFP signal (green) was present in the cytosol, not overlapping with the plastid autofluorescence (PAF, red) (Figure 3A). By contrast, in the *NoPDAT-eGFP* transformants, the green eGFP signal formed irregular layers surrounding the plastid (red) (Figure 3B), which was further supported by a three-dimensional visualization of eGFP and PAF signals (Figure 3C). We also introduced the *NoPDAT-eGFP* fusion into *Phaeodactylum tricornutum*, a Heterokont alga with bigger cells, in which there is experimental demonstration of cER-localized proteins (Hempel et al., 2009). Clearly, the eGFP signal (green) surrounded the plastid (red) and nucleus (blue, stained with Hoechst) (Figure 3D), resembling the localization pattern of hDer1-2, a confirmed cER-localized protein (Hempel et al., 2009). These results suggest that NoPDAT resides at the cER.

Overexpression of *NoPDAT* in *N. oceanica* Promotes TAG Accumulation without Compromised Growth and Suggests a Consumption of 16:0 and 16:1 in Polar Lipids

To investigate the function and biological role of *NoPDAT* in *N. oceanica*, we first generated overexpressing lines. The wild-type (WT) strain was used as control. More than ten putative transformants (confirmed by genomic PCR) were screened by quantitative real-time PCR (qPCR). Two lines, PDAT-OE3 and PDAT-OE5 that showed maximal increase in *NoPDAT* transcripts (>10-fold higher than WT), were selected for subsequent analysis (Figure 4A). Immunoblot analysis using the NoPDAT antibody revealed that NoPDAT protein abundance was higher in the two transformants than in WT (Figure 4B). During a 10-day batch culture period, no difference in the culture

optical density (OD_{730}) was observed between the transformants and WT (Figure 4C), suggesting that *NoPDAT* overexpression had no effect on the growth of *N. oceanica*. Accordingly, the nitrate concentration in the culture medium showed no difference between the transformants and WT and was almost consumed within six days (Figure 4D). Fluorescence intensity assay of Nile red-stained algal cells, a rapid and reliable method for relative TAG quantification in algae (Ge et al., 2014; Li et al., 2019), indicated that *N. oceanica* accumulated TAG after four days of culture and the transformants had a higher TAG content than WT during the late culture days (days 6-10; Figure 4E). Gas chromatography–mass spectrometry (GC–MS) quantification revealed that *NoPDGT* overexpression enhanced TAG by ~32%, yet having no consequences on the content in total FA (TFA) (Figure 4F). *NoPDAT* overexpression had a limited effect on the FA profile of TAG, whereas a slight decrease of 16:0 and 16:1 and increase of 20:5 was noticed in TFA (Figure 4G and 4H). Since the FA profile in TFA accounts for both membrane lipids and TAG, and since the percentage of TAG within this proportion increases, the impact on TFA, even minor, reflects a consumption of 16:0 and 16:1 in polar lipids. Therefore, it can be hypothesized that NoPDAT mainly transfers 16:0 and 16:1 from polar lipids *in vivo*. We sought to confirm this deduction by analyzing mutants defective in NoPDAT expression.

Knockdown of *NoPDAT* Attenuates TAG Accumulation and Decreases the Proportion of TAG with 16:0 and 16:1 at *sn*-3 Position

We generated *NoPDAT* knockdown lines of *N. oceanica* via RNAi-mediated gene-silencing. Two out of more than ten putative transformants, PDAT-KD2 and PDAT-KD4 that had the lowest *NoPDAT* transcript abundance (<10% of that in WT on day 8), were chosen for subsequent experiments (Figure 5A). Similar to the overexpression, *NoPDAT* knockdown had little impact on the growth of *N. oceanica* (Figure 5B). Nile red staining

and fluorescence intensity assay indicated that the knockdown lines had a TAG content lower than WT, particularly during the late culture days (Figure 5C). GC–MS quantification confirmed the decrease in TAG (reduced by ~32%) caused by *NoPDAT* knockdown, whereas TFA content showed little change (Figure 5D). Concerning FA profiles, *NoPDAT* knockdown increased the relative abundance of 16:0 and 16:1 and decreased that of 18:1, 20:4 and C20:5 in TFA; by contrast the FA profile of TAG remained apparently unchanged compared to the WT (Figure 5E and 5F). Assuming that TFA reflects FA contained in membrane lipids and TAG, the differences observed in TFA should reflect an impact on membrane glycerolipids. Thus, a knockdown of NoPDAT clearly leads to the accumulation of 16:0 and 16:1 in membrane glycerolipids.

To uncover the *NoPDAT* knockdown-associated global changes of TAG species in a time-resolved manner, TAG quantification by electrospray ionization mass spectrometry (ESI–MS) analysis was conducted, using the samples of WT and PDAT-KD4 cells from three time points, *i.e.* day 3, day 5 and day 7. There was no difference in total TAG content between PDAT-KD4 and WT on day 3, a time point before TAG accumulation in *N. oceanica* cells; by contrast, PDAT-KD4 showed a significantly lower total TAG content than WT on day 5 and day 7 (Figure 6). These results suggest that in *N. oceanica*, NoPDAT is not involved in the production of a basal level of TAG under favorable growth conditions, but likely acts under nutrient stress, opposite to the function of *C. reinhardtii* PDAT that contributes more to basal TAG biosynthesis than for TAG accumulation in stationary phase (Yoon et al., 2012).

More than 50 TAG molecular species were identified in *N. oceanica*, shown in Figure 6 and supplemental Data set 1. Among them, seven molecular species, *i.e.* 52:6 (20:5/16:0/16:1), 50:3 (16:1/18:1/16:1), 50:2 (16:0/16:1/18:1), 48:3 (16:1/16:1/16:1), 48:2 (16:1/16:1/16:0), 48:1 (16:1/16:0/16:0), 46:2 (14:0/16:1/16:1), and 46:1 (16:1/16:0/14:0), accounted for more than 70% of total TAG in both WT and PDAT-KD4

cells on day 3. It is important to notice that PDAT can transfer acyl groups finally recorded at the *sn*-1 or *sn*-3 positions of TAG. Over time (e.g., on day 5 and day 7), most of the TAG species followed a similar accumulation pattern and increased considerably in WT and PDAT-KD4. Albeit having no impact on total TAG content in *N. oceanica* on day 3, *NoPDAT* knockdown modulated the content of individual TAG species, which were not initially visible when simply considering the TAG FA profile. Focusing on the seven main molecular species, those whose proportion decreased, *i.e.* (16:1/16:1/16:1), (16:1/16:1/16:0), (14:0/16:1/16:1) and (16:1/16:0/14:0), were more specifically impacted by the knockdown of NoPDAT, highlighting mainly a defect in transfer of 16:0 and 16:1 at position *sn*-3. At day 3, this trend was also observed for minor TAG species and conversely, the proportion of TAG species containing 20:4 or 20:5 at positions *sn*-1 or *sn*-3 increased. At day 5, all TAG species showed a significant decrease in the *NoPDAT* knockdown lines, consistent with a lowering of the TAG production, and the capacity of NoPDAT to transfer other acyls than 16:0 or 16:1. We sought whether some glycerolipids exhibited a change in their FA that could mirror the decrease in 16:0 and 16:1 in TAG, by a balanced accumulation.

Knockdown of *NoPDAT* Leads to an Accumulation of PE and PG Enriched in 16:0, 16:1 and 18:1

PDAT mediates the acyl-CoA independent TAG biosynthesis in which membrane glycerolipids are used as acyl donors (Dahlqvist et al., 2000). We sought whether a specific lipid class accumulated in the *NoPDAT* knockdown strains compared to WT, based on semi-quantitative TLC analysis of polar lipids, after staining of resolved lipids by iodine. One band clearly accumulated in the KD lines (Figure 7A-left). This band was recovered, subjected to mass spectrometry analysis, and characterized as PE enriched in saturated or monounsatured FA. Henceforth, the TLC spot characterized by such PE

molecular species is referred to as “less-unsaturated PE” or LU-PE.

Quantification via ESI–MS analysis was then conducted for WT and PDAT-KD4 cultures harvested on day 3, day 5, and day 7 under air condition. WT showed a decrease in the overall PE content in the course of cultivation (Figure 7B) and the PE profile was predominantly more-unsaturated, with 20:4/20:4, 20:5/20:4, 20:4/20:3, and 20:5/20:5 accounting for over 80% of PE (Figure 7C), consistent with previous observation in *Nannochloropsis* species (Nobusawa et al., 2017; Alboresi et al., 2016). In PDAT-KD4, the consumption of PE was arrested (Figure 7B). Thus, although NoPDAT had no apparent activity on PE in *in vitro* enzymatic assay (Figure 2C), PDAT-KD4 accumulated a much higher level of this membrane lipid than the WT (~2.2 fold) regardless of the culture time points (Figure 7B). In PDAT-KD4, the molecular species of PE, which showed an accumulation, were those detected by TLC, i.e. 16:0/16:1 (>100-fold higher than that in WT), followed by 16:1/18:1, 16:1/16:1, 16:0/18:1, 16:0/16:0, 14:0/16:0 and 14:0/16:1 (Figure 7C), corresponding to LU-PE. Considering the *sn*-2 position in LU-PE molecular species, PE appears therefore as a major donor of 16:0, 16:1 and 18:1, for NoPDAT action.

Since *in vitro* assays support the capacity of NoPDAT to use other acyl donors, we examined other lipid classes. In line with the strong *in vitro* activity of NoPDAT on PG (Figure 2C), the PDAT-KD4 line was marked by a ~80% higher level of this lipid class compared to the WT, at all time points (Figure 7B). A total of eight PG species were detected, and like for PE, those harboring a 16:0 or 16:1 at position *sn*-2 accumulated in the PDAT-KD4 line (Figure 7D). However, different from PE that tended to increase in PDAT-KD4 line, PG decreased gradually in both WT and PDAT-KD4 cells as the culture persisted.

Minor quantitative variations were noticeable for phospholipids such as PC or PI (Figure 7B), consistent with *in vitro* tests (Figure 2C). However, contrary to the results

obtained with plastid glycolipids in *in vitro* assays, MGDG or DGDG levels changed a little in the PDAT-KD4 line compared to the WT (Figure 7B). As for the FA profiles of MGDG, DGDG or PC, a slight enrichment in molecular species measured in the PDAT-KD4 line concerned 16:0 or 16:1 at the *sn*-2 position, which could be related to a utilization by NoPDAT (Supplemental Figure 2). These findings suggest that NoPDAT may have poor activity on PC, PI, MGDG or DGDG in *in vivo* conditions, either by a lack of specificity or due to a location of the enzyme with limited access to these lipids. Interestingly, in the course of cultivation, the WT strain showed some variations in the PC profile, such as a decrease in molecular species with a 16:1 at the *sn*-2 position, balanced by an increase of molecular species enriched in 18:1 or 18:2, but these changes were unaffected by the *NoPDAT* knockdown, and are therefore unrelated to this enzyme. DGTS relative quantity was evaluated based on the staining intensity on TLC plate, showing no moderate change except for day 3 in the PDAT-KD4 line (Supplemental Figure 3).

Eventually, plasmenylethanolamine (PME) was detected in trace amount in *N. oceanica* and accumulated considerably (~15 fold) following *NoPDAT* knockdown, showing that this unusual phospholipid, structurally close to PE, could also serve as acyl donor for NoPDAT (Figure 7E).

Transcriptional Response of Lipid Metabolic Genes to *NoPDAT* Knockdown

To investigate the effect of *NoPDAT* knockdown on lipid metabolism network at the transcriptional level, reverse-transcription qPCR (RT-qPCR) was conducted for 55 lipid metabolic genes in WT and PDAT-KD4 (Figure 8 and supplemental Data set 2). The pyruvate dehydrogenase (PDH) that catalyzes the production of acetyl-CoA, the enzymes involved in *de novo* fatty acid biosynthesis such as acetyl-CoA carboxylase (ACC), malonyl-CoA:ACP transacylase (MCAT), ketoacyl-ACP synthase III and I

(KASIII/KASI), ketoacyl-ACP reductase (KAR), hydroxyacyl-ACP dehydrase (HAD), and enoyl-ACP reductase (ENR), acyl-ACP desaturase (AAD) that is responsible for the formation of $16:1^{\Delta7}$-ACP and $18:1^{\Delta9}$-ACP, and long-chain acyl-CoA synthetase 2 (LACS2) that catalyzes the production of acyl-CoA pool were down-regulated at the transcriptional level in response to *NoPDAT* knockdown. Since *NoPDAT* knockdown attenuates TAG biosynthesis (Figure 5D and Figure 6), it is likely that the cellular demand for FAs is lower, giving rise to a transcriptional down-regulation feedback on FA biosynthesis (Figure 8). In line with this, PDAT-KD4 had a slightly lower TFA content than WT (Figure 5D).

The Δ6-fatty acid desaturase (Δ6 FAD) that introduces a double bond between carbons 6 and 7 on C18 acyls and fatty acid elongase 2 (FAE2) that catalyzes the formation of C20 acyls from C18 acyls were also down-regulated in the *NoPDAT* knockdown line (Figure 8). This may partially explain that the knockdown strains had lower percentage of very long-chain fatty acids 20:4 and 20:5 (Figure 5E).

When considering enzymes involved in the Kennedy pathway, the expression of GPAT, LPAT1, LPAT2, LPAT3, LPAT4 and of DGATs was little impacted. This indicates that a lack of NoPDAT does not trigger any compensatory mechanism via the acyl-CoA dependent pathway, consistent with the observed impact of overexpression and knockdown on TAG levels. The PDAT pathway appears therefore independent from the Kennedy pathway.

Finally, although PE, PG and PME increased considerably (Figure 7), no up-regulation of their biosynthesis at the transcriptional was observed in response to *NoPDAT* knockdown (Figure 8). Altogether, the analysis of the transcription of lipid metabolism genes suggests an orchestrated control of FA production, but no clear reprograming of genes involved in membrane lipid or TAG assembly. The phenotype of *NoPDAT* knockdown line observed at the level of lipid classes is therefore mainly attributable to a

regulation of the metabolic network, and not to a long term genetic reprogramming.

CO_2 Availability Affects the *NoPDAT* Knockdown-Associated Accumulation of PE Enriched in 16:0, 16:1 and 18:1

The accumulation of LU-PE was observed in *NoPDAT* knockdown cultures aerated with air and was visible by TLC analysis (Figure 7A-left), however, it was absent in PDAT-KD4 line grown at static condition (Figure 7A-right). For the WT, the LU-PE band was not visible even with the aeration of 2% CO_2 until day 7 (Supplemental Figure 4A), let alone the static (Supplemental Figure 3) and air conditions (Figure 7A-left). Accordingly, PDAT-KD4 aerated with 2% CO_2 accumulated more LU-PE than air condition as shown on TLC plate (Figure 7A-right).

To gain the detailed changes in response to CO_2 availability, quantification of glycerolipids in PDAT-KD4 via ESI–MS was performed. Compared to cultures aerated with air, static cultures showed a higher level of glycolipids (MGDG and DGDG) but a lower level of phospholipids (PG, PE, PC and PI); Cultures aerated with 2% CO_2, on the other hand, was comparable to cultures aerated with air in the level of MGDG, DGDG and PG, yet having a higher level of PE and PI and a lower level of PC (Figure 7B). Unlike those PE enriched in 20:4/20:4, 20:5/20:4 and 20:4/20:3 that had the highest level in cultures aerated with air, LU-PE species were all correlated with the CO_2 availability and their levels followed the order of static cultures <cultures aerated with air< cultures aerated with 2% CO_2 (Figure 7C). Similarly, the PG enriched in 16:0, 16:1 and 18:1 in PDAT-KD4 were positively correlated with CO_2 availability (Figure 7D). PME species were also increased by CO_2 availability: the higher CO_2 supply, the higher level of PME (Figure 7E). In addition, the level of some more-unsaturated MGDG and DGDG species was lower in cultures aerated with air than that in static cultures (Supplemental Figure 2). Under static condition, LU-PE maintained a rather low level in PDAT-KD4 line on day 5,

though it was higher than that on day 5 in WT aerated with air. Moreover, LU-PE content of PDAT-KD4 under static condition was comparable to that on day 3 and less than a half of that on day 7 in WT aerated with air, and it was less than 10% and 5% of that of PDAT-KD4 aerated with air and 2% CO_2 respectively.

PDAT mRNA level increased in the course of cultivating and maintained the highest from day 5 to 7 at air condition in WT (Supplemental Figure 4B), and immunoblotting analysis showed that increasing CO_2 supply (from air to 2% and 5% CO_2) in the culture enhanced PDAT expression (Supplemental Figure 4C). It was evident that accumulation of LU-PE in WT cells either at day 7 or with elevated CO_2 supply was not attributed to the down-regulated PDAT, showing that LU-PE may act as carbon sink under stress with high CO_2 level. In fact, aeration with 5% CO_2 led to a visible LU-PE band not only in WT but also in PDAT overexpression strains (Supplemental Figure 4A).

Although TAG species responded differentially to CO_2 availability in PDAT-KD4, the major more-unsaturated TAG species such as 52:6 (20:5/16:0/16:1), 52:5 (20:4/16:1/16:0) and 52:4 (20:3/16:0/16:1) were correlated with CO_2 supply and their levels followed the order of static cultures <cultures aerated with air< cultures aerated with 2% CO_2 (Figure 6). These data suggest under high CO_2 supply conditions, acyl-donors with 16:0 and 16:1 are likely partitioned preferentially to PE (maybe also PG) while acyl-donors with 20:4 and 20:5 are partitioned preferentially to TAG, with LU-PE and TAG serving as carbon sinks.

LU-PE Accumulation is Independent from Genes Involved in PE Homeostasis

The analysis of the *NoPDAT* knockdown line suggests that this enzyme is responsible for the specific consumption of PE with 16:0 and 16:1 at position *sn*-2 of molecular species, collectively called LU-PE, which then represent a minor proportion of PE molecular species. We wondered whether the molecular specificity of other enzymes involved in the

production or catabolism of PE could also control LU-PE. We performed overexpression and/or knockdown of a series of genes (Figure 9), including those encoding a putative plant-type DAG:CDP-alcohol (choline/ethanolamine) phosphotransferase (CPT/EPT), a bifunctional enzyme responsible for the last biosynthetic step of PE and PC in the Kennedy pathway, a base-exchange-type phosphatidylserine synthase (PSS) that converts PE into PS, a phosphatidylethanolamine *N*-methyltransferase (PEMT) and a phospholipid *N*-methyltransferase (PLMT) that catalyze the methylation of PE to form PC, and phosphoethanolamine *N*-methyltransferase (PEAMT) that converts phosphoethanolamine to phosphocholine for subsequent PC synthesis (Han et al., 2017; Li-Beisson et al., 2019; Zienkiewicz et al., 2020). One-dimension TLC was used to screen phenotypes, based on the detection of the specific LU-PE band, used as readout. Overexpressing of each of the two *CPT*/*EPT* genes did not induce any accumulation of LU-PE in *N. oceanica* (Supplemental Figure 5). The turnover of LU-PE species is therefore unlikely counterbalanced by an increase in PE production. Likewise, overexpression of *PSS* or knockdown of *PSS*, *PEMT*, *PLMT* or *PEAMT* did not lead to any LU-PE accumulation (Supplemental Figure 5). Altogether, these results indicated that LU-PE accumulation in *N. oceanica* is not linked to the genes involved in PE homeostasis, and that NoPDAT is solely responsible for the observed profile change.

DISCUSSION

NoPDAT is a Canonical Glycerolipid:Diacylglycerol Acyltransferase, with a Broad Spectrum of Possible Acyl-Donors, Using Mainly PG and PE *in vivo*

N. oceanica is able to accumulate high levels of TAG, probably due to the presence of a great number of acyltransferases involved in TAG biosynthesis, namely, thirteen DGATs and one PDAT (Vieler et al., 2012b; Wang et al., 2014). Only three out of the six DGATs and the PDAT from *C. reinhardtii* have been shown to restore TAG synthesis in TAG-

deficient yeast (Yoon et al., 2012; Hung et al., 2013; Liu et al., 2016a). By contrast, in addition to the PDAT (Figure 2), six DGATs from *N. oceanica* have been proven to enable TAG synthesis in the same species (Wei et al., 2017a; Xin et al., 2017, 2019). *C. reinhardtii* PDAT showed a lower *in vitro* TAG-synthesizing activity than DGATs (Yoon et al., 2012; Liu et al., 2016a). *N. oceanica* PDAT, on the other hand, seemed more active than DGATs in *in vitro* TAG synthesis (Figure 2; Wei et al., 2017a; Xin et al., 2017). While DGATs use acyl-CoAs, PDATs transfer acyl groups already esterified to a lipid donor. Since the early characterization utilized PC for investigating *in vitro* PDAT activities, the enzyme was named as phospholipid:diacylglycerol acyltransferase (Dahlqvist et al., 2000). In fact, PDATs can utilize not only phospholipids but many other substrates as acyl donors, yet the activity and substrate preference are dependent on the PDAT sources (Dahlqvist et al., 2000; Yoon et al., 2012; Feng et al., 2019). Both *S. cerevisiae* and Arabidopsis PDATs preferentially transfer the acyl at the *sn*-2 position of PC and PE to the *sn*-3 position of DAG to form TAG (Dahlqvist et al., 2000; Ghosal et al., 2007; Fan et al., 2013a, 2013b; Feng et al., 2019). Concerning *C. reinhardtii*, the *in vitro* analysis of CrPDAT highlighted distinct levels of activity and substrate preference, when using various truncated forms of the enzyme, supporting that PDAT conformation, insertion into a membrane, and exposure of hydrophobic residues were critical for interaction with potential substrates. Thus, CrPDAT substrate preference evaluated with a truncated form, highlighted a higher activity with anionicacyl-donors, such as PG, and a lower activity using zwitterionic lipids such as PE and PC (Yoon et al., 2012). When evaluating MGDG, DGDG or SQDG as possible acyl donors, only MGDG could be used as substrate for CrPDAT, but this *in vitro* activity could be only detected with a full-length version of the enzyme (Yoon et al., 2012). Here, *N. oceanica* PDAT had no detectable activity on PE or PC, but exhibited an apparent *in vitro* preference for PG, and to some extent MGDG, DGDG or SQDG, reminiscent to the results obtained with the *C.*

reinhardtii enzyme (Figure 2C). It must be noticed that the lipidic substrates, obtained from commercial suppliers, contained molecular species differing from those occurring naturally in *N. oceanica*. On the acceptor side, NoPDAT was efficient on a broad series of DAG molecular species, suggesting that this enzyme could potentially function with a variety of substrates.

As the analyses of overexpression and knockdown lines supported that LU-PE, harboring 16:0, 16:1 or 18:1 at position *sn*-2, were natural acyl-donors for NoPDAT (Figure 7C), we tested additional PE species, but none of them proved to be utilized by the enzyme in the *in vitro* conditions (Supplemental Figure 6). Similarly, *N. oceanica* PDAT exhibits no observed *in vitro* activity on PC regardless of the acyl compositions (Supplemental Figure 6). Noteworthy, when PG was used as the acyl donor, *N. oceanica* PDAT showed a consistent preference for molecular species harboring 16:0 and 16:1 at the *sn*-2 position in *in vitro* conditions (Supplemental Figure 6).

Considering all *in vitro* and *in vivo* results, we thus demonstrated that NoPDAT is a canonical glycerolipid:diacylglycerol acyltransferase, which can accept a broad range of acyl-donors with 16:0, 16:1 and to some extent 18:1 at position *sn*-2, transferred to DAG. *In vivo*, main substrates appear to be PE and PG.

The substrate variation of PDATs may also arise from their diversification during evolution. Green and red algae (Chlorophyta and Rhodophyta) originated from a primary endosymbiosis, whereas Stramenopile/Heterokonts emerged from a secondary endosymbiosis, in which eukaryotic hosts engulf and retain a red alga (McFadden et al., 2001; Yoon et al., 2002; Maréchal, 2018; Fussy and Obornik, 2018). Although both *N. oceanica* and *P. tricornutum* belong to Heterokont algae, the balance between secondary host vs endosymbiont genetic importance differed over the course of speciation. In *N. oceanica*, the symbiont nucleus likely dominated over the host nucleus, whereas in *P. trocornutum* the symbiont nucleus was probably discarded (Guo et al., 2019). It is

possible that *N. oceanica* and *P. tricornutum* PDATs were inherited from the symbiont and host nuclei, respectively. Consistent with this hypothesis, the PDAT sequences from Eustigmatophytes and Bacillariophyceae did not group together in reconstructed phylogenetic tree (Figure 1). It has been proposed that PDATs evolution could be driven by different selection constraints and that positive selection may play critical roles in PDAT function (Falarz et al., 2020). Certain amino acids under positive selection within the 'lid' region and adjacent to the catalytic serine (designated by the red arrows; Supplemental Figure 1) are probably involved in this diversification of PDAT structure and function. More functional data need to be gathered in the Heterokont/Stramenopile phylum to investigate this hypothesis.

N. oceanica PDAT Contributes to Membrane Lipid Turnover during Stress-Induced TAG Biosynthesis

In the batch cultures performed in the present work, wild-type *N. oceanica* showed a rapid growth within the first four days and then the algal growth slowed down, indicative of the onset of nutrient limitation stress (Figure 4C and Figure 5B). Consistently, the nitrate content monitored in the culture medium was drastically consumed within the first four days (Figure 4D) and thereafter TAG began to accumulate (Figure 4E and Figure 5C). Neither *NoPDAT* overexpression nor *NoPDAT* knockdown caused any important change in TAG content of *N. oceanica* before day 4, thus considered as the favorable growth (nutrient replete) condition with a basal level of synthesized TAG (Figures 4-6). By contrast, after four days of cultivation, when the algal cells were exposed to nutrients' limitation, a striking increase of TAG was observed in *NoPDAT* overexpressing lines, and an opposite trend was observed in *NoPDAT* knockdown lines (Figures 4-6). These results suggest a significant contribution of NoPDAT to TAG production at the onset of the stationary phase. In line with this deduction, in the WT background, the *NoPDAT*

transcripts showed a regular increase on day 5 and day 8 compared to day 2 (Figure 4A and Figure 5A). In this context, NoPDAT may function as a TAG contributor in *N. oceanica* under stress conditions, but not under favorable fast-growing conditions, differing from *C. reinhardtii* or *S. cerevisiae* in which PDAT contributes mainly to TAG accumulation under favorable growth conditions (Oelkers et al., 2002; Yoon et al., 2012). Nevertheless, the analysis of knockdown lines showed that even in early cultivation stages, the acyl-donors of PDAT, *i.e.*LU-PE, accumulated. In addition, we observed a decrease of several TAG species caused by *NoPDAT* knockdown on day 3, though the total TAG level showed little change (Figure 6). Thus, we cannot rule out the possibility that NoPDAT operates on a basal level and contributes to non-stress associated TAG synthesis as well, but not detectable compared to the bulk produced via the Kennedy pathway, as several *NoDGAT* genes have been demonstrated to contribute mainly to TAG biosynthesis in *N. oceanica* under non-stress conditions (Wei et al., 2017a; Xin et al., 2017, 2019). Moreover, NoPDAT, resembling CrPDAT that harbors a conserved lipase motif and can hydrolase various lipids (Supplemental Figure 1; Yoon et al., 2012), may not only transfer acyl moieties from membrane lipids to DAG for TAG biosynthesis but act only as a lipase, as suggested by the increase of many membrane lipids on day 3 in response to *NoPDAT* knockdown (Figure 7B).

Parallel and Possibly Independent TAG Productions via NoPDAT and NoDGAT Pathways

Of the three *N. oceanica DGAT* genes that function mainly under stress conditions, knockdown of *NoDGAT1A*, *NoDGAT2A* and *NoDGAT2D* leads to TAG decrease by 25%, 26% and 47%, respectively (Wei et al., 2017a; Xin et al., 2017). In the present study, *NoPDAT* knockdown caused ~38% decrease in TAG level (Figure 5D). Thus, although these experiments were not strictly conducted under the same conditions and the gene

knockdown efficiencies may vary, NoPDAT likely makes a comparable contribution to stress-induced TAG accumulation as each of the above-mentioned NoDGATs. It is worth noting that, if summing up the TAG decrease ratios caused by silencing each of the four acyltransferase genes in *N. oceanica*, the value exceeds 100%. In this context, these acyltansferases may have overlapping roles. The interactions between enzymes involved in TAG synthesis including DGAT and PDAT have been reported in mammals (Man et al., 2006; Jin et al., 2014), land plants (Lee and Seo, 2019; Xu et al., 2019a) and algae (Xu et al., 2019b). In Arabidopsis, "oil-producing metabolons" were recently characterized, containing either DGAT1 or DGAT2 and PDAT, with accesses to separate substrate pools (Regmi et al., 2020). It would be important to evaluate whether similar metabolons might occur in such a species with so many oil-producing enzymes. In our study, we noticed little impact on the expression of genes coding for NoGPAT, NoLPATs and NoDGATs in response to a knockdown of NoPDAT (Figure 8). Only a down-tuning of FA synthetic genes seemed to occur.

Altogether, NoPDAT is likely to operate as a parallel and independent oil-producing route, possibly dispensable to feed an actual form of carbon storage, and more important as an actor of membrane lipid turnover (Yoon et al., 2012; Fan et al., 2013b, 2014). The occurrence of such PDAT-mediated membrane lipid turnover in *N. oceanica* is further supported by several lines of evidence. First, as the culture time lasted (from favorable growth to nutrient limitation stress), *NoPDAT* showed a steady increase in its transcript level (Figure 4A, Figure 5A and Supplemental Figure 4B), accompanied by the decrease of many membrane lipids (Figure 7B). Second, following *NoPDAT* knockdown, membrane lipids particularly PG and PE exhibited a considerable increase regardless of the culture time points examined (Figure 7B). The increase of PG particularly PG with 16:0, 16:1 and 18:1 at the *sn*-2 position caused by *NoPDAT* knockdown is in agreement with the *in vitro* enzymatic assay results that NoPDAT exhibited a stronger activity on

these PG species (Figure 7D; Supplemental Figure 6). The impact on PE level is even more evident.

NoPDAT Location at the cER Highlights the Presence of Both PG and PE in the Outermost Membrane of the Plastid

There are two possible origins for CDP-diacylglycerol-glycerol-3-phosphate 3-phosphatidyltransferase (or phosphatidylglycerolphosphate synthase, PGPS) producing PG. One is prokaryotic, at the origin of the plastid PGPS in Archeplastida, and the other is eukaryotic, for PGPS in the mitochondrion (Luévano-Martínez, 2015). The situation in Heterokont has not been established. Based on sequence similarity search, both types are encountered. We could identify one sequence in *N. oceanica* (Nanoce1779|7997, in the CCMP1779 genome) related to prokaryotic PGPS, harboring both signal peptide and chloroplastic transit sequences together with an ASAFAP motif, indicating that a prokaryotic-like PGPS is likely to synthesize PG in the plastid. Homologues were also detected in *M. gaditana* (EKU22790 in CCMP526) and *P. tricornutum* (Phatr3_J8663). We could also identify one sequence related to eukaryotic PGPS in *M. gaditana* (EKU20337), *P. tricornutum* (Phatr3_J47576) and a C-terminal fragment in *N. oceanica* (Nanoce1779|6370). A mitochondrial transit peptide is predicted using MitoprotII for Phatr3_J47576 and EKU20337, which suggests that these eukaryotic-type PGPS produce PG in the mitochondrion. Eventually, PG might also be exported to the endomembrane system, via inter-organellar transport (Vance, 2015), via a protein machinery which remains to be characterized. In *N. oceanica* profile we cannot unambiguously assess which of the detected PG molecular species is mitochondrial and/or plastidial or even in the ER. Although there is no information available about the distribution of PG in *N. oceanica*, the predominance of C16 acyls over C18 acyls in PG *sn*-2 position (Figure 7D) suggests that *N. oceanica* synthesizes the bulk of its PG in the chloroplast. Considering

the subcellular localization of NoPDAT at the cER (Figure 3), it could possibly access PG from both the ER (low abundance) and the plastid outer envelope. NoPDAT may not use PG species located at the thylakoid membrane or the chloroplast inner envelope *per se*, unless this lipid is translocated to the cER, which needs to be assumed to interpret the knockdown phenotype.

PE represents a major non-bilayer phospholipid widely distributed in the extra-chloroplastic membranes of Archaeplastida. It is believed that PE biosynthesis involves mainly two metabolic pathways, *i.e.*, an ER-localized CDP-ethanolamine pathway (*de novo* biosynthetic pathway) and a mitochondrial PS decarboxylation pathway, with the former being the major one (Gibellini and Smith, 2010). In *N. oceanica*, PE is present predominantly in the form of molecular species with no less than four double bonds (Figure 7C; Li et al., 2014b; Han et al., 2017; Meng et al., 2017). Based on our analysis of genes involved in the biosynthesis or conversion of PE, the produced LU-PE was mainly consumed by cER NoPDAT to form TAG and otherwise accumulated, and could not be converted to PE enriched in 20:3, 20:4 and 20:5. The cER thus appears as a major membrane lipid remodeling site, during long nutrient stress, marked by a consumption of PE and PG molecular species.

LU-PE serves as an alternative carbon reservoir in *N. oceanica* under stress

Since LU-PE species are the acyl-donors for NoPDAT, knockdown of *NoPDAT* could result in LU-PE accumulation, which is boosted by elevated CO_2 supply. It is suggested that LU-PE may serve as an alternative yet essential carbon reservoir for photosynthetically assimilated carbon. The large pool of LU-PE is produced in response to nutrient limitation when TAG biosynthesis is impaired or under high CO_2 conditions, which indicated a potential protection mechanism in cells under stress. The protective role of LU-PE is further supported as there's no difference between the growth rate of

WT and *NoPDAT* knockdown lines under stress, despite lower TAG content in the latter. By contrast, knockdown of *PDAT* and knockout of *plastid galactoglycerolipid degradation 1* gene (*pgd1*) in *C. reinhardtii* decreased cellular TAG content and their growth rates in the mid-exponential growth phase and stationary phase under stress, respectively (Li et al., 2012; Yoon et al., 2012), supporting a role of TAG in protecting algal cells against oxidative damage. In *NoPDAT* knockdown lines, this protective role appears to be replaced by accumulation of LU-PE as an alternative electron and carbon sink against overreduction of photosynthetic electron transport chain and possibility production of reactive oxygen species under stress.

Considering that PE enriched in 20:3, 20:4 and 20:5 showed no increase while LU-PE rose drastically (Figure 7C), the fatty acid elongases and desaturases (Han et al., 2017; Poliner et al., 2018a) may not function on the acyl groups of those LU-PE species in *N. oceanica* (Figure 9). Due to the greatly different acyl-chain length and unsaturation of LU-PE, if the vastly increased LU-PE species are transported to the biologically functional two-layer membranes, the membrane structure and function would be changed. To avoid such a drastic change, LU-PE species may be stored on the monolayer of lipid droplets, which generally occur in algal cytosol under stress conditions to accommodate TAG (Wang et al., 2009; Vieler et al., 2012a; Wang et al., 2019). More researches are to be carried out to identify the location and function of LU-PE in cells in the future.

CONCLUSIONS

The remarkably high content of TAG in *N. oceanica* has been attributed to the strongly redundant equipment of NoDGATs. This is absolutely plausible, since some are more expressed and active in favorable growth conditions and others during severe nutrient limitations. Based on these assumptions, the function of *NoPDAT* might appear as dispensable. Interestingly, in the *NoPDAT* knockdown lines, no compensatory

mechanisms via the Kennedy pathway could be observed, neither by metabolic regulation, which could fill up the cell with oil to the same level as the WT, nor via transcriptional reprogramming, by overexpression of *GPAT*, *LPATs* or *DGATs*. All results support that the PDAT pathway is a parallel and independent oil-producing pathway. This role in coupling membrane glycerolipid breakdown at the periphery of the plastid, mainly via PG and PE, with TAG production, is likely one of the features determining the remarkable capacity of *Nannochloropsis* species to accumulate such high levels of TAG. It may be part of the mechanisms adjusting membrane lipids with the cellular physiological status, here during a long nutrient stress. In particular, the specific saturated/monounsaturated acyl PE, accumulating under stress, is a substitute for TAG to respond quickly and directly to the excessive carbon flux. The activation of the PDAT pathway now needs to be evaluated in various physiological and environmental contexts to route the specific PE to TAG effectively. Such feature should be also useful for future strategies aiming at further improving the production of TAG by genetic engineering of *Nannochloropis* and related species.

METHODS

Algal Strains

Nannochloropsis oceanica (MBIC10090) and *Phaeodactylum tricornutum* (CCMP2561) were obtained from the Marine Biotechnology Institute Culture Collection (Iwate, Japan) and the culture collection of the Provasoli-Guillard National Center for Culture of Marine Phytoplankton (Maine, USA) respectively. Algal cultures were grown axenically in artificial seawater enriched with f/2 nutrients (nitrate concentration was reduced to 500 µM) (Guillard, 1975) at 22 °C under continuous illumination of 120 µmol photons m^{-2} s^{-1}. Transformants were grown in medium with the presence of 1 (for *N. oceanica*) or 40 µg/ml (for *P. tricornutum*) zeocin.

Identification of Putative *PDAT* Encoding Gene in *N. oceanica* and Phylogenetic Analyses

Since the annotation of *PDAT* in JGI *Nannochloropsis oceanica* CCMP1779 v1.0 (*Protein ID 11464* and *Protein ID 1202*) and v2.0 (*Protein ID 530913*) are different, and the transcript of *Protein ID 530913* overlaps partial transcripts of *Protein ID 11464* and *Protein ID 1202*. Protein ID 530913 contains all the conserved regions ('lid' region, salt bridge and catalytic S-D-H triad) of PDAT (Falarz et al., 2020), while Protein ID 11464 contains only the PDAT 'lid' region and Protein ID 1202 contains incomplete catalytic triad (Asp and His). To obtain the correct full-length cDNA of *N. oceanica PDAT* (*NoPDAT*), three primer pairs were designed based on the three annotated gene sequences and three DNA fragments amplified from the cDNA template were obtained. The obtained long fragment not only included one of the short fragments but also is overlapped with the 3' end of the other. The full-length cDNA of this gene was further verified by 3' and 5'-RACE. The latest annotation information in JGI *Nannochloropsis oceanica* CCMP1779 v2.0 on the Protein ID 640709 issues its full-length, which is the same with that obtained in our experiment (Supplemental Figure 7). The full-length coding regions of *NoPDAT* were amplified by using *N. oceanica* cDNA as template with the primer pair *11464-fw* and *1202-rv*. Total RNA was extracted with TRIzol reagent (Invitrogen) from exponentially growing cells homogenized by grinding in liquid nitrogen. DNA was removed with gDNA Eraser and first-strand cDNA was synthesized by PrimeScript RT reagent Kit (TaKaRa) according to the manufacturer's instructions. All the primers are shown in Supplementary Data set 3.

For phylogenetic analyses, a final dataset composed of 30 sequences (see supplementary method) was aligned using MUSCLE (Edgar, 2004) then curated using BMGE (Block Mapping and Gathering with Entropy) software (Criscuolo and Gribaldo,

2010) to select the phylogenetic informative regions. The Le-Gascuel (Le and Gascuel, 2008) substitution model for Maximum Likelihood (ML) phylogenetic inference method was chosen among the 56 models implemented in MEGA X (Kumar et al., 2018) (Molecular Evolutionary Genetics Analyses) software as the model best fitting the dataset. A Maximum Likelihood phylogenetic analysis was hence performed on the curated alignment with LG+G+I model and 5000 bootstrap pseudo-replicates (details of the analyses are presented in supplementary method). A Bayesian phylogenetic inference was carried out as well. Two independent Metropolis-coupling Markov Chain Monte Carlo analyses were performed using the MrBayes3.2 (Ronquist et al., 2012) software (details in the supplementary method).

NoPDAT Expression in Yeast

The open reading frame (ORF) of NoPDAT was cloned into the yeast expression vector pYES2-CT (Invitrogen). The resulting vectors pYES2-NoPDAT was confirmed by restriction digestion and sequencing. The recombinant pYES2-NoPDAT plasmid was then transformed into the *Saccharomyces cerevisiae* TAG-deficient quadruple mutant strain H1246 (*dga1*, *lro1*, *are1*, and *are2*) by using S.c. EasyComp Transformation Kit (Invitrogen). Transformants were selected on solid plates of SC-uracil medium (Teknova, Hollister, CA, USA). H1246 cells carrying the empty plasmid pYES2-CT (EV control) and pYES2-CrDGTT3 (a type 2 *DGAT* gene from *Chlamydomonas reinhardtii*) were from Liu et al. (2016a). Yeast cells were grown in SC-uracil medium with 2% raffinose for 24 hours. Cells were harvested by centrifugation at 1,500 × g for 5 min and resuspended in SC-uracil medium containing 2% galactose with an initial OD_{600} of 0.4 for induction. After the induction of 2 days, total lipids from yeast cells were extracted as described by Yoon et al. (2012) and neutral lipids were separated on a Silica gel 60 thin layer chromatography (TLC) plate (EMD Chemicals, Merck, Darmstadt, Germany) using

a mixture of hexane/tert-butylmethyl ether/acetic acid (80/20/2, by volume) as the mobile phase. Lipids were detected by spraying the TLC plate with 10% $CuSO_4$ in 8% phosphoric acid, followed by charring at 180°C for 3 min. BODIPY 493/503 (Invitrogen), a neutral lipid-specific fluorescent dye, was used for the staining of yeast cells.

Yeast Microsome Preparation and *in vitro* PDAT Activity Assay

The transformant cells of H1246 bearing pYES2-NoPDAT were grown in SC-uracil medium with 2% galactose for 12 h at 30°C. Cells were then harvested and washed twice with ice-cold distilled water. The cell pellets were resuspended in cell lysis buffer (containing 5% glycerol, 20 mM Tris-HCl (pH 8.0), 0.3 M ammonium sulfate, 10 mM $MgCl_2$, 1 mM EDTA, 1 mM DTT, 1× EDTA-free protease inhibitor cocktail set X (Calbiochem), 1 mM PMSF) to an OD_{600} of approximately 100 and lysed by passing twice through a French pressure cell (Spectronics Instruments, Rochester, NY, USA) at an internal pressure of 15,000 PSI. Cell debris was removed from the suspension by centrifugation at 10,000 × g for 10 min at 4°C and the supernatant was centrifuged further at 100,000 × g for 2 h at 4°C. The resulting microsomal membrane pellets were resuspended in microsome storage buffer (50 mM Tris-HCl, pH 7.5, 10% glycerol) to give a protein concentration of 10 μg μL^{-1} for immediate use or stored at -80 °C.

The *in vitro* PDAT assay was conducted according to our previously described procedures (Liu et al., 2016a). The polar lipids tested included 1,2-dipalmitoyl-sn-glycero-3-O-4'-[N,N,N-trimethyl(d9)]-homoserine (DGTS), 1-palmitoyl-2-oleoyl-sn-glycero-3-phosphocholine (PC), 1-palmitoyl-2-oleoyl-sn-glycero-3-phosphoethanolamine (PE), 1-palmitoyl-2-oleoyl-sn-glycero-3-phospho-(1'-rac-glycerol) (PG), 1-palmitoyl-2-oleoyl-sn-glycero-3-phospho-L-serine (PS), digalactosyldiacylglycerol (DGDG, plant sourced), phosphatidylinositol (PI, soy sourced), 1-palmitoyl-2-oleoyl-sn-glycero-3-

phosphate (PA), monogalactosyldiacylglycerol (MGDG, plant sourced), sulphoquinovosyldiglyceride (SQDG, plant sourced), and the diacylglycerols (DAGs) were 16:0/16:0, 16:1/16:1, 18:1/16:0, 16:0/18:1, 18:1/18:1, 1,3-18:1/18:1, 18:2/18:2, and 18:3n3/18:3n3. 16:1/16:1, 18:2/18:2, and 18:3n3/18:3n3 DAGs, and SQDG were purchased from Larodan Fine Chemicals (Malmo, Sweden), whereas 18:1/16:0 DAG was prepared by partial digestion of 18:1/16:0/18:1 triacylglycerol (TAG) (Larodan Fine Chemicals) with *Rhizopus arrhizus* lipase (Sigma-Aldrich) and recovery of DAG. All other lipids were purchased from Avanti Polar Lipids (Alabaster, AL, USA).

GFP Fusion and Overxpression Constructs

For the localization analysis of NoPDAT, two constructs were generated to express C-terminal enhanced green fluorescent protein (eGFP) fusion proteins in *N. oceanica* and *P. tricornutum* cells respectively. NoPDAT ORF was amplified by PCR using primers *nopdat_pP-EcoRI-fw* and *nopdat-KpnI-rv* and inserted into the *Kpn* I-*Eco*R I sites (upstream of the *eGFP* sequence) of the pPhaT1-eGFP vector (Zhang and Hu, 2014), to generate the pPhaT1-NoPDAT-eGFP vector. Plasmid pPha-NoVCPp containing the endogenous bidirectional *N. oceanica violaxanthin/chlorophyll a-binding protein 2* (*NoVCP2*) promoter and *NOVCP1* 3'UTR (terminator) as well as *sh ble* resistance gene was constructed according to Moog et al. (2015) and has been described in our previous study (Chen and Hu, 2019). NoPDAT ORF was amplified using primer pair *nopdat_KpnI-fw* and *nopdat-XbaI-rv* and ligated into the pPha-NoVCPp (between the *Kpn* I and *Xba* I sites), to obtain *NoPDAT* overexpression vector pPha-NoVCPp-NoPDAT. To generate the pPha-NoVCPp-NoPDAT-eGFP vector, *eGFP* was cloned and inserted downstream of the *NoVCP2* promoter of pPha-NoVCPp (Chen and Hu, 2019), then the PCR product amplified by primers *nopdat_KpnI-fw* and *nopdat-KpnI-rv* was digested and cloned into the *Kpn* I site of the vector pPha-NoVCPp-eGFP. Inserts of all

constructs were sequenced to confirm that no mutations were present. *Hpa* I linearized pPhaT1-NoPDAT-eGFP was introduced into wild-type *P. tricornutum*, and *Hpa* I linearized pPha-NoVCPp-NoPDAT and pPha-NoVCPp-NoPDAT-eGFP were respectively introduced into wild-type *N. oceanica* following our previous protocol (Zhang and Hu, 2014; Li et al., 2014a). The transformants were screened by PCR for the presence of transgene using specific primers. GFP positive cells were observed using a Leica TCS SP8 laser scanning confocal microscope. Chlorophyll autofluorescence and GFP fluorescence were excited at 488 nm, and were detected with 630–690 nm and 500–550 nm, respectively. Fluorescence of the nucleus stained by Hoechst 33342 was detected at 425–475 nm emission by 405 nm excitation. NoPDAT overexpression in *N. oceanica* was confirmed by quantitative real-time PCR (qPCR) and western blot analysis.

For the overexpression of *choline phosphotransferase* (*CPT*, *Protein ID 9914*), *ethanolamine phosphotransferase* (*EPT*, *Protein ID 8504*) and *phosphatidylserine synthase* (*PSS Protein ID 6823*) in *N. oceanica*, their ORFs were amplified using primer pairs *nocpt_KpnI-fw* and *nocpt-XbaI-rv*, *noept_KpnI-fw* and *noept-XbaI-rv*, and *nopss_KpnI-fw* and *nopss-XbaI-rv* respectively, then ligated into the pPha-NoVCPp vector. Before being transformed into wild-type *N. oceanica*, the overexpression vectors were linearized with *Hpa* I (EPT-OE and PSS-OE vectors) or *Sca*I (CPT-OE vector) and then purified with DNA purification kit according to our previous method (Li et al., 2014a).

Quantitative Real-Time PCR and Western Blot Analysis

Total RNA was extracted from algal cells at different growth phases and cDNA was prepared as mentioned above. Relative gene expression was measured using the SsoAdvanced Universal SYBR Green Supermix (Bio-Rad) and aLightCycler 480 Real-Time PCR System (Roche). Primers used for real-time PCR are shown in Supplementary

Data set 3. *Histone H4* served as the internal control gene (Siaut et al., 2007). Technical triplicates were performed for duplicate cultures. The mean values of relative mRNA quantities were calculated according to the $2^{-\Delta\Delta Ct}$-method.

For the western blot analysis, total protein was extracted from liquid nitrogen-frozen algal cells in RIPA lysis buffer containing 1 mM phenylmethanesulfonyl fluoride (Beyotime Biotechnology, China) by ultrasonication for 10 min at 10% intensity (5 s duration, 5 s intervals, on ice using Scientz JY96-IIN Sonifier). Extracts were centrifuged and protein concentration in the supernatant was determined using a BCA protein assay kit (Beyotime Biotechnology, China). After denaturation, total protein was separated by 10% SDS-PAGE gel and then transferred to polyvinylidene fluoride membrane. The membranes were incubated with anti-NoPDAT antibody followed by HRP-conjugated secondary antibody and the blots were developed with Immobilon Western Chemiluminescent HRP Substrate (Millipore, USA). Images of the blots were obtained using an ImageQuant LAS 4000 mini apparatus (GE Healthcare Life Science). Polyclonal antibody of NoPDAT was generated by Genscript Corporation (Nanjing, China) against a synthetic peptide CPHLEKETGTFSSEE.

Growth and Nile Red Staining

Growth was determined by measuring the optical density (OD) at 750 nm and the initial inoculation density is OD_{750}=0.05. Nitrate concentration in the culture was determined using spectrophotometry at 220 nm (Collos et al., 1999). The relative abundance of the algal neutral lipid was estimated by fluorescence spectroscopy (Perkin-Elmer, LS 55) with the fluorescent dye Nile red (Sigma-Aldrich) using procedures described before (Ge et al., 2014) with some modification. Briefly, a total of 0.5 OD cell suspensions were harvested by centrifugation, and 500 μl of 70% ethanol was added to resuspend cell pellets. The resuspended solution was subject to incubation at 4°C for 10 min, and were

subsequently incubated at 37°C for 30 min after addition of 2.5 ml of ddH_2O and 30 µl of 100 µg/ml Nile red solution. Fluorescent emission was measured at 572 nm with an excitation wavelength of 531 nm. Background fluorescence for this filter set was subtracted prior to the addition of Nile red.

Total Lipid and TAG Content Analysis of *N. oceanica*

Total lipids of algal cells were extracted in a chloroform/methanol (1:1, v/v) solvent system (Bligh and Dyer, 1959) and were further separated by TLC on Silica gel plates 60 using hexane/diethyl ether/acetic acid (70:30:1, v/v/v) as developing solvent (Reiser and Somerville, 1997). TAGs were identified by staining with iodine vapor and recovered with methanol from the plates. Triolein was used as the standard and was purchased from Sigma-Aldrich. Total lipids and TAGs were transesterified with 1 M sulfuric acid in methanol at 100°C for 1 h. Fatty acid methyl esters from the transesterification of total lipids and TAGs were analyzed by gas chromatography (TRACE GC; Thermo Scientific) and quantified using methylheptadecanoate (C17:0) as the internal standard following our previously described procedures (Ge et al., 2014).

Construction of RNAi Strains

To silence *NoPDAT* in *N. oceanica*, a hairpin construct was built using the primer pairs *nopdat535_fw* and *nopdat975_rv1* for 'long' fragment (LF), and *nopdat535_fw* and *nopdat761_rv2* for 'short' fragment (SF) following our previous methods (Wei et al., 2017b). After linearization with *Sca* I, the hairpin construct driven by the native *β-tubulin* promoter was introduced into wild-type *N. oceanica* according to the procedure described by Li et al. (2014a). The transformants were screened by checking the integration of the *sh ble* gene with the primers *ble_fw* and *ble_rv*.

To construct RNAi expression vector for *PSS*, *phosphatidylethanolamine N-*

methyltransferase (*PEMT*), *phospholipid N-methyltransferase* (*PLMT*) and *phosphoethanolamine N-methyltransferase* (*PEAMT*), primer pairs *pss344_fw* and *pss739_rv1*, *pemt229_fw* and *pemt630_rv1*, *plmt102_fw* and *plmt524_rv1*, *peamt652_fw* and *peamt1051_rv1* were used for LF amplification, and primer pairs *pss344_fw* and *pss554_rv2*, *pemt229_fw* and *pemt429_rv2*, *plmt102_fw* and *plmt314_rv2*, *peamt652_fw* and *peamt871_rv2* were used for SF amplification. Prior to transformation to wild-type *N. oceanica*, the four RNAi vectors were linearized using *Sca* I (*PEMT*, *PLMT* and *PEAMT*-RNAi vector) or *Kpn* I (*PSS*-RNAi vector).

TAG Molecular Composition and Content

TAG molecular composition and content were analyzed as described previously (Hu et al., 2014; Ge et al., 2014). In brief, TAGs recovered from TLC plates as mentioned above were redissolved in chloroform/methanol (1:1, v/v). The TAG samples were dried and dissolved in isopropanol, and then were analyzed by a Shimadzu LC-20AD HPLC system coupled with an AB 4000 Q trap tandem MS system (Applied Biosystems, USA) using APCI in positive mode. A ZORBAX Eclipse Plus phenyl-hexyl column (4.6 mm × 250 mm i. d., 5μm particle size, Agilent Technologies, USA) was used for the separation, and mobile phase was consisted of acetonitrile (solvent A) and 0.5% ammonia-methanol (w/v) (solvent B) in gradient elution mode. For the elution, 50% of solution B was used during first 7.5 min. Then a gradient from 50% to 72% of solution B was supplied during next 0.5 min with an isocratic hold at 72% for additional 5 min, then 72% to 50% in 0.1 min, followed by an isocratic hold at 50% for 17 min. The injection volume was 10 μL, with flow rate = 0.8 mL/min. The heated interface temperature, curtain gas pressure and collision gas were set to 450 °C, 30 psi and medium respectively. The EMS (enhanced MS) – EPI (Enhanced Product Ion) scan mode was applied for qualitative analysis, and the MRM (multiple reaction monitoring) – EPI mode was used for quantification. The

scan rate was 1000 μ/s, and the ion source gas 1 pressure was set at 45 psi. The declustering potential and the collision energy were set at 84 and 35±15 V, respectively. Scan range of the EMS was set at m/z 700–1000, and the EPI at m/z 100–1000.

Qualitative and Quantitative Analysis of Polar Lipids

Total lipid extracts and polar lipid standards were subjected to TLC as above in a solvent system consisting of chloroform/methanol/acetic acid/distilled water (75:13:9:3 v/v/v/v). The standards of MGDG, PE, PG, PC, PS, PI purchased from Avanti Polar Lipids (Alabama, USA) were used to identify the classes of polar lipids on the plates. Furthermore, each band on the plates was scraped off respectively, and the silica gel powder was extracted with methanol and dried, then redissolved in chloroform/methanol (1:1, v/v). The redissolved single lipids were identified using shotgun MS approach according to Wei et al. (2018). In addition, total lipids extracted from wild-type and *NoPDAT* knockdown strains were also analyzed using shotgun MS method directly. For the shotgun MS method, an Shimadzu LC-20AD HPLC system and an AB 4000 Q trap tandem MS system (Applied Biosystems, USA) with an electrospray ionization (ESI) source in positive-ion mode were used. The ionization voltages were set to 5 kV. The ion source temperature (TEM), curtain gas (CUR) and ion source gas 1 (GS1) were set to 350 °C, 10 psi and 16 psi, respectively.The flow rate of the sample injected into the ESI source was set to 20 μL/min.The declustering potential (DP) of PC (+PIS 184), PE (+NLS 141), PS (+NLS 185), PG (+NLS 189), PA (+NLS 115), PI (+NLS 277), MGDG (+NLS 179), and DGDG (+NLS 341) were set to 166.8, 139.9, 127.7, 64.6, 71.3, 120.4, 86.3, and 73 V, respectively, and the collision energy (CE) was set to 47.7, 35.3 , 38.8, 28.5, 25.7, 32.6, 20.2, and 23.7 V respectively. The MS scan was from 400 to 1000 m/z. PC (12:0/12:0), PE (12:0/12:0), PS (14:0/14:0), PG (14:0/14:0), PA (14:0/14:0) and PI (8:0/8:0) were used as internal standards for quantification of phospholipids (PLs).

MGDG and DGDG were quantified by external standard method using PE. The fatty acid compositions of PLs were analyzed by EPI scanning in negative-ion mode using manual tuning. Data acquisition and processing were performed using AB SCIEX Analyst 1.5 Software (Applied Biosystems, Foster City, CA, USA).

Statistical Analysis

Statistical analysis was performed using the SPSS Statistics 20.0 software. Data were expressed as mean ± SD (standard deviation) based on three independent biological replicates. Two-tailed Student's *t* tests (*t* test) were performed to determine statistical significance, and the threshold was set at 0.05 or 0.01.

Supplemental Data

The following materials are available in the online version of this article.

Supplemental Figure 1. Sequence alignment of the amino acids of phospholipid:diacylglycerol acyltransferase (PDAT). The seven most characteristically conserved domains are shown and predicated transmembrane domain in *Nannochloropsis oceanica* PDAT (NoPDAT) are boxed. AtPDAT1, *Arabidopsis thaliana* PDAT1; AtPDAT2, *A. thaliana* PDAT2; ScPDAT, *Saccharomyces cerevisiae* PDAT; PtPDAT, *Phaeodactylum tricornutum* PDAT; TpPDAT, *Thalassiosira pseudonana* PDAT; NgPDAT, *Nannochloropsis gaditana*. Arrows indicate catalytic triad (Ser-Asp-His).

Supplemental Figure 2. Content of MGDG, DGDG and PC species in wild-type (WT) and the *NoPDAT* knockdown line (PDAT-KD4) of *Nannochloropsis oceanica*. Static, static culture; Air, culture aerated with air; CO_2, culture aerated with 2% CO_2. Data represent mean ± SD (n=3).

Supplemental Figure 3. Effect of *NoPDAT* knockdown on DGTS of *Nannochloropsis oceanica* as determined by TLC analysis (the abundance of wild-type on day 3 was set as

1). Static, static culture; Air, culture aerated with air; CO_2, culture aerated with 2% CO_2. Data represent mean ± SD (*n*=3). WT, wild-type; PDAT-KD4, *NoPDAT* knockdown line 4.

Supplemental Figure 4. Effect of culture conditions on LU-PE accumulation (A), *NoPDAT* mRNA (B, determined by qPCR) and protein (C, determined by immunoblotting) levels in wild-type (WT), *NoPDAT* knockdown (PDAT-KD2 and PDAT-KD4) and overexpression lines (PDAT-OE3 and PDAT-OE5) of *Nannochloropsis oceanica*. Static, static culture; Air, culture aerated with air; 2% CO_2, culture aerated with 2% CO_2; 5% CO_2, culture aerated with 5% CO_2. MU-PE: "more-unsaturated PE", PE enriched in 20:3, 20:4 and 20:5 fatty acids; LU-PE: "less-unsaturated PE", PE enriched in saturated or monounsatured fatty acids. The *NoPDAT* mRNA levels under air condition at 36 h (B, left) or under static condition (B, right, dot line) was set as 1.

Supplemental Figure 5. Effect of *CPT* overexpression (CPT-OE1~6), *EPT* overexpression (EPT-OE1~5), *PEMT* knockdown (PEMT-KD2, 4~8), *PLMT* knockdown (PLMT-KD1~6), *PEAMT* knockdown (PEAMT-KD3, 5), *PSS* knockdown (PSS-KD8, 11) and *PSS* overexpression (PSS-OE14, 15) on LU-PE accumulation in *N. oceanica*. MU-PE: "more-unsaturated PE", PE enriched in 20:3, 20:4 and 20:5 fatty acids; LU-PE: "less-unsaturated PE", PE enriched in saturated or monounsatured fatty acids.

Supplemental Figure 6. *In vitro* assay of NoPDAT on PE, PC and PG with various acyl compositions.

Supplemental Figure 7. Gene structures of the *Nannochloropsis oceanica PDAT* annotated in JGI v1 (11464, 1202) and v2 (530913, 640709).

Supplemental Data Set 1. Contents (nmol/mg dry biomass) of TAG species and the values of fold change shown in the heat map of Figure 6.

Supplemental Data Set 2. The values of fold change in transcript levels of genes encoding components involved in lipid metabolism.

Supplemental Data Set 3. Primers used in this study for qPCR, RNAi expression vector, overexpression vector and GFP fusion vector construction.

Supplemental Method. Phylogenetic analyses on PDAT datasets

ACKNOWLEDGMENTS

This work was supported by the National Natural Science Foundation of China (41976119, 91751117). A.A., E.M., H.H. and Y.G. were supported by a CEA-CAS bilateral program. J.L. was supported by the National Key R&D Program of China (2018YFA0902500). A.A. and E.M. were supported by the French National Research Agency (GRAL Labex ANR-10-LABEX-04, and EUR CBS ANR-17-EURE-0003).

AUTHOR CONTRIBUTIONS

H.H. conceived and designed the research. J.Y., Y.P. and T.H. performed the *in vivo* experiments. J.L designed the *in vitro* experiments in yeast and performed them with M.L. A.A. contributed the phylogenetic analyses. H.H., J.L., J.Y., Y.P. and Y.G. analyzed the data. J.L. and H.H. drafted the manuscript. E.M., Y.L., J.L., A.A. and H.H. made critical revision. All authors read and approved the final article.

References

Alboresi, A., Perin, G., Vitulo, N., Diretto, G., Block, M., Jouhet, J., Meneghesso, A., Valle, G., Giuliano, G., Maréchal, E., and Morosinotto, T. (2016). Light remodels lipid biosynthesis in *Nannochloropsis gaditana* by modulating carbon partitioning between organelles. Plant Physiol. **171:** 2468–2482.

Armenteros, J.J.A., Salvatore, M., Emanuelsson, O., Winther, O., von Heijne, G., Elofsson, A., and Nielsen, H. (2019). Detecting sequence signals in targeting peptides using deep learning. Life Sci. Alliance **2:** e201900429.

Bligh, E.G., and Dyer, W.J. (1959). A rapid method of lipid extraction and purification. Can. J. Biochem. Physiol. **37:** 911–917.

Boyle, N.R., Page, M.D., Liu, B., Blaby, I.K., Casero, D., Kropat, J., Cokus, S.J., Hong-Hermesdorf, A., Shaw, J., Karpowicz, S.J., Gallaher, S.D., Johnson, S., Benning, C., Pellegrini, M., Grossman, A., and Merchant, S.S. (2012). Three acyltransferases and nitrogen-responsive regulator are implicated in nitrogen starvation-induced triacylglycerol accumulation in *Chlamydomonas*. J. Biol. Chem. **287:** 15811–15825.

Chapman, K.D., and Ohlrogge, J.B. (2012). Compartmentation of triacylglycerol accumulation in plants. J. Biol. Chem. **287:** 2288–2294.

Chen, Y., and Hu, H. (2019). High efficiency transformation by electroporation of the freshwater alga *Nannochloropsis limnetica*. World J. Microb. Biot. **35:** 119.

Claros, M.G., Vincens, P. (1996). Computational method to predict mitochondrially imported proteins and their targeting sequences. Eur. J. Biochem. **241:** 770–786.

Collos, Y., Mornet, F., Sciandra, A., Waser, N., Larson, A., and Harrison, P.J. (1999). An optical method for the rapid measurement of micromolar concentrations of nitrate in marine phytoplankton cultures. J. Appl. Phycol. **11:** 179–184.

Criscuolo, A., and Gribaldo, S. (2010). BMGE (Block Mapping and Gathering with

Entropy): a new software for selection of phylogenetic informative regions from multiple sequence alignments. BMC Evol. Biol. **10:** 210.

Dahlqvist, A., Ståhl, U., Lenman, M., Banaś, A., Lee, M., Sandager, L., Ronne, H., and Stymne, S. (2000). Phospholipid:diacylglycerol acyltransferase: an enzyme that catalyzes the acyl-CoA-independent formation of triacylglycerol in yeast and plants. Proc. Natl. Acad. Sci. USA **97:** 6487–6492.

Dolch, L.J., Rak, C., Perin, G., Tourcier, G., Broughton, R., Leterrier, M., Morosinotto, T., Tellier, F., Faure, J.D., Falconet, D., Jouhet, J., Sayanova, O., Beaudoin, F., and Maréchal, E. (2017). A palmitic acid elongase affects eicosapentaenoic acid and plastidial monogalactosyldiacylglycerol levels in *Nannochloropsis*. Plant Physiol. **173:** 742–759.

Edgar, R.C. (2004). MUSCLE: multiple sequence alignment with high accuracy and high throughput. Nucleic Acids Res. **32:** 1792–1797.

Falarz, L.J., Xu, Y., Caldo, K.M.P., Garroway, C.J., Singer, S.D., and Chen, G. (2020). Characterization of the diversification of phospholipid:diacylglycerol acyltransferases in the green lineage. Plant J. **103:** 2025–2038.

Fan, J., Yan, C., and Xu, C. (2013a). Phospholipid:diacylglycerol acyltransferase-mediated triacylglycerol biosynthesis is crucial for protection against fatty acid-induced cell death in growing tissues of Arabidopsis. Plant J. **76:** 930–942.

Fan, J., Yan, C., Roston, R., Shanklin, J., and Xu, C. (2014). *Arabidopsis* lipins, PDAT1 acyltransferase, and SDP1 triacylglycerol lipase synergistically direct fatty acids toward β-oxidation, thereby maintaining membrane lipid homeostasis. Plant cell **26:** 4119-4134.

Fan, J., Yan, C., Zhang, X., and Xu, C. (2013b). Dual role for phospholipid:diacylglycerol acyltransferase: enhancing fatty acid synthesis and diverting fatty acids from membrane lipids to triacylglycerol in *Arabidopsis* leaves.

Plant Cell **25:** 3506–3518.

Fawley, M.W., Jameson, I., and Fawley, K.P. (2015). The phylogeny of the genus *Nannochloropsis* (Monodopsidaceae, Eustigmatophyceae), with descriptions of *N. australis sp. nov.* and *Microchloropsis gen. nov*. Phycologia **54:** 545–552.

Feng, Y., Zhang, Y., Ding, W., Wu, P., Cao, X., and Xue, S. (2019). Expanding of phospholipid:diacylglycerol acyltransferase (PDAT) from *Saccharomyces cerevisiae* as multifunctional biocatalyst with broad acyl donor/acceptor selectivity. Appl. Biochem. Biotechnol. **88:** 824–835.

Flori, S., Jouneau, P.H., Finazzi, G., Maréchal, E, and Falconet, D. (2016). Ultrastructure of the periplastidial compartment of the diatom *Phaeodactylum tricornutum*. Protist. **167:** 254-67.

Füssy, Z., and Oborník, M. (2018). Complex endosymbioses I: from primary to complex plastids, multiple independent events. Methods Mol. Biol. **1829:** 17–35.

Ge, F., Huang, W., Chen, Z., Zhang, C., Xiong, Q., Bowler, C., Yang, J., Xu, J., and Hu, H. (2014). Methylcrotonyl-CoA carboxylase regulates triacylglycerol accumulation in the model diatom *Phaeodactylum tricornutum*. Plant Cell **26:** 1681–1697.

Ghosal, A., Banaś, A., Ståhl, U., Dahlqvist, A., Lindqvist, Y., and Stymne, S. (2007). *Saccharomyces cerevisiae* phospholipid:diacylglycerol acyl transferase (PDAT) devoid of its membrane anchor region is a soluble and active enzyme retaining its substrate specificities. Biochim. Biophys. Acta **1771:** 1457–1463.

Gibbs, S.P. (1979). The route of entry of cytoplasmically synthesized proteins into chloroplasts of algae possessing chloroplast ER. J. Cell Sci. **35:** 253–266.

Gibellini, F., and Smith, T.K. (2010). The Kennedy pathway—De novo synthesis of phosphatidylethanolamine and phosphatidylcholine. IUBMB Life **62:** 414-428.

Glukhova, A., Hinkovska-Galcheva, V., Kelly, R., Abe, A., Shayman, J.A., and

Tesmer, J.J. (2015). Structure and function of lysosomal phospholipase A 2 and lecithin:cholesterol acyltransferase. Nat. Commun. **6:** 6250.

Gschloessl, B., Guermeur, Y., and Cock, J. M. (2008). HECTAR: a method to predict subcellular targeting in heterokonts. BMC Bioinform. **9:** 393.

Guillard, R.R.L. (1975). Culture of phytoplankton for feeding marine invertebrates. In Culture of Marine Invertebrate Animals, W.L. Smith and M.H. Canley, eds (New York: Plenum Press), pp. 29–60.

Guo, L., Liang, S., Zhang, Z., Liu, H., Wang, S., Pan, K., Xu, J., Ren, X., Pei, S., and Yang, G. (2019). Genome assembly of *Nannochloropsis oceanica* provides evidence of host nucleus overthrow by the symbiont nucleus during speciation. Commun. Biol. **2:** 249.

Han, D., Jia, J., Li, J., Sommerfeld, M., Xu, J., and Hu, Q. (2017). Metabolic remodeling of membrane glycerolipids in the microalga *Nannochloropsis oceanica* under nitrogen deprivation. Front. Mar. Sci. **4**.

Hempel, F., Bullmann, L., Lau, J., Zauner, S., and Maier, U.G. (2009). ERAD-derived preprotein transport across the second outermost plastid membrane of diatoms. Mol. Biol. Evol. **26:** 1781–1790.

Hori, K., Maruyama, F., Fujisawa, T., Togashi, T., Yamamoto, N., Seo, M., Sato, S., Yamada, T., Mori, H., Tajima, N., Moriyama, T., Ikeuchi, M., Watanabe, M., Wada, H., Kobayashi, K., Saito, M., Masuda, T., Sasaki-Sekimoto, Y., Mashiguchi, K., Awai, K., Shimojima, M., Masuda, S., Iwai, M., Nobusawa, T., Narise, T., Kondo, S., Saito, H., Sato, R., Murakawa, M., Ihara, Y., Oshima-Yamada, Y., Ohtaka, K., Satoh, M., Sonobe, K., Ishii, M., Ohtani, R., Kanamori-Sato, M., Honoki, R., Miyazaki, D., Mochizuki, H., Umetsu, J., Higashi, K., Shibata, D., Kamiya, Y., Sato, N., Nakamura, Y., Tabata, S., Ida, S., Kurokawa, and K., Ohta, H. (2014). *Klebsormidium flaccidum* genome reveals primary factors for plant

terrestrial adaptation. Nat. Commun. **5:** 3978.

Hu, N., Wei, F., Lv, X., Wu, L., Dong, X.-Y., and Chen, H. (2014). Profiling of triacylglycerols in plant oils by high-performance liquid chromatography–atmosphere pressure chemical ionization mass spectrometry using a novel mixed-mode column. J. Chromatogr. B. **972:** 65–72.

Hung, C.-H., Ho, M.-Y., Kanehara, K., and Nakamura, Y. (2013). Functional study of diacylglycerol acyltransferase type 2 family in *Chlamydomonas reinhardtii*. Febs Lett **587:** 2364-2370.

Jin, Y., McFie, P.J., Banman, S.L., Brandt, C., and Stone, S.J. (2014). Diacylglycerol acyltransferase-2 (DGAT2) and monoacylglycerol acyltransferase-2 (MGAT2) interact to promote triacylglycerol synthesis. J Biol Chem **289:** 28237-28248.

Kelly, L.A., Mezulis, S., Yates, C., Wass, M., and Sternberg, M. (2015). The Phyre2 web portal for protein modelling, prediction, and analysis. Nat. Protoc. **10:** 845–858.

Kim, H.U., Lee, K.R., Go, Y.S., Jung, J.H., Suh, M.C., and Kim, J.B. (2011). Endoplasmic reticulum-located PDAT1-2 from castor bean enhances hydroxy fatty acid accumulation in transgenic plants. Plant Cell Physiol **52:** 983-993.

Krogh, A., Larsson, B., von Heijne, G., and Sonnhammer, E.L.L. (2001). Predicting transmembrane protein topology with a hidden markov model: Application to complete genomes. J. Mol. Biol. **305:** 567–580.

Kumar, S., Stecher, G., Li, M., Knyaz, C., and Tamura, K. (2018). MEGA X: Molecular evolutionary genetics analysis across computing platforms. Mol. Biol. Evol. **35:** 1547–1549.

Le, S.Q., and Gascuel, O. (2008). An improved general amino acid replacement matrix. Mol. Biol. Evol. **25:** 1307–1320.

Lee, H.G., and Seo, P.J. (2019). Interaction of DGAT1 and PDAT1 to enhance TAG assembly in *Arabidopsis*. Plant Signal Behav. **14:** 1554467.

Lee, J., Ghosh, S., and Saier, M.H. (2017). Comparative genomic analyses of transport proteins encoded within the red algae *Chondrus crispus*, *Galdieria sulphuraria*, and *Cyanidioschyzon merolae*. J. Phycol. **53:** 503–521.

Li, D.-W., Balamurugan, S., Yang, Y.-F., Zheng, J.-W., Huang, D., Zou, L.-G., Yang, W.-D., Liu, J.-S., Guan, Y., and Li, H.-Y. (2019). Transcriptional regulation of microalgae for concurrent lipid overproduction and secretion. Sci. Adv. **5:** eaau3795.

Li, F., Gao, D., and Hu, H. (2014a). High-efficiency nuclear transformation of the oleaginous marine *Nannochloropsis* species using PCR product. Biosci. Biotech. Bioch. **78:** 812–817.

Li, J., Han, D., Wang, D., Ning, K., Jia, J., Wei, L., Jing, X., Huang, S., Chen, J., Li, Y., Hu, Q., and Xu, J. (2014b). Choreography of transcriptomes and lipidomes of *Nannochloropsis* reveals the mechanisms of oil synthesis in microalgae. Plant Cell **26:** 1645–1665.

Li, X., Moellering, E.R., Liu, B., Johnny, C., Fedewa, M., Sears, B.B., Kuo, M.-H., and Benning C. (2012). A galactoglycerolipid lipase is required for triacylglycerol accumulation and survival following nitrogen deprivation in Chlamydomonas reinhardtii. Plant Cell **24:** 4670–4686.

Li-Beisson, Y., Thelen, J.J., Fedosejevs, E., and Harwood, J.L. (2019). The lipid biochemistry of eukaryotic algae. Prog. Lipid Res. **74:** 31-68.

Liu, J., Han, D., Yoon, K., Hu, Q., and Li, Y. (2016a). Characterization of type 2 diacylglycerol acyltransferases in *Chlamydomonas reinhardtii* reveals their distinct substrate specificities and functions in triacylglycerol biosynthesis. Plant J. **86:** 3–19.

Liu, J., Lee, Y-Y., Mao, X., and Li, Y. (2017). A simple and reproducible non-radiolabeled in vitro assay for recombinant acyltransferases involved in triacylglycerol biosynthesis. J. Appl. Phycol. **29:** 323–333.

Liu, X.-Y., Ouyang, L.-L., and Zhou, Z.-G. (2016b). Phospholipid: diacylglycerol acyltransferase contributes to the conversion of membrane lipids into triacylglycerol in *Myrmecia incisa* during the nitrogen starvation stress. Sci. Rep. **6:** 26610–26610.

Luévano-Martínez, L.A. (2015). The chimeric origin of the cardiolipin biosynthetic pathway in the Eukarya domain. Biochim. Biophys. Acta. **1847:** 599–606.

Ma, X.-N., Chen, T.-P., Yang, B., Liu, J., and Chen, F. (2016). Lipid production from *Nannochloropsis*. Mar. Drugs **14:** 61.

Man, W.C., Miyazaki, M., Chu, K., and Ntambi, J. (2006). Colocalization of SCD1 and DGAT2: implying preference for endogenous monounsaturated fatty acids in triglyceride synthesis. J. Lipid Res. **47:** 1928-1939.

Mao, X., Wu, T., Kou, Y., Shi, Y., Zhang, Y., and Liu, J. (2019). Characterization of type I and type II diacylglycerol acyltransferases from the emerging model alga *Chlorella zofingiensis* reveals their functional complementarity and engineering potential. Biotechnol. Biofuels **12:** 28.

Maréchal, E. (2018). Primary endosymbiosis: emergence of the primary chloroplast and the chromatophore, two independent events. Methods Mol. Biol. **1829:** 3–16.

McFadden, G.I. (2001). Primary and secondary endosymbiosis and the origin of plastids. J. Phycol. **37:** 951-959.

Meng, Y., Cao, X., Yao, C., Xue, S., and Yang, Q. (2017). Identification of the role of polar glycerolipids in lipid metabolism and their acyl attribution for TAG accumulation in Nannochloropsis oceanica. Algal Res. **24, Part A:** 122-129.

Mhaske, V., Beldjilali, K., Ohlrogge, J., and Pollard, M. (2005). Isolation and characterization of an *Arabidopsis thaliana* knockout line for phospholipid:diacylglycerol transacylase gene (At5g13640). Plant Physiol. Biochem. **43:** 413–417.

Moog, D., Stork, S., Reislöhner, S., Grosche, C., and Maier, U-G. (2015). In vivo

localization studies in the stramenopile alga *Nannochloropsis oceanica*. Protist. **166:** 161–171.

Mori, N., Moriyama, T., Toyoshima, M., and Sato, N. (2016). Construction of global acyl lipid metabolic map by comparative genomics and subcellular localization analysis in the red alga *Cyanidioschyzon merolae*. Front. Plant Sci. **7:** 958.

Nielsen, H., Tsirigos, K.D., Brunak, S., and von Heijne, G. (2019). A Brief history of protein sorting prediction. Protein J. **38:** 200–216.

Nobusawa, T., Hori, K., Mori, H., Kurokawa, K., and Ohta, H. (2017). Differently localized lysophosphatidic acid acyltransferases crucial for triacylglycerol biosynthesis in the oleaginous alga *Nannochloropsis*. Plant J. **90:** 547–559.

Oelkers, P., Cromley, D., Padamsee, M., Billheimer, J.T., and Sturley, S.L. (2002). The *DGA1* gene determines a second triglyceride synthetic pathway in yeast. J. Biol. Chem. **277:** 8877–8881.

Oelkers, P., Tinkelenberg, A., Erdeniz, N., Cromley, D., Billheimer, J.T., and Sturley, S.L. (2000). A lecithin cholesterol acyltransferase-like gene mediates diacylglycerol esterification in yeast. J. Biol. Chem. **275:** 15609–15612.

Pan, X., Peng, F.Y., and Weselake, R.J. (2015). Genome-wide analysis of *Phospholipid-diacylglycerol acyltransferase (PDAT)* genes in plants reveals the eudicot-wide PDAT gene expansion and altered selective pressures acting on the core eudicot *PDAT* paralogs. Plant Physiol. **167:** 887–904.

Petroutsos, D., Amiar, S., Abida, H., Dolch, L.J., Bastien, O., Rébeillé, F., Jouhet, J., Falconet, D., Block, M.A, McFadden, G.I., Bowler, C., Botté, C., and Maréchal, E. (2014). Evolution of galactoglycerolipid biosynthetic pathways – From cyanobacteria to primary plastids and from primary to secondary plastids. Prog. Lipid Res. **54:** 68–85.

Poliner, E., Clark, E., Cummings, C., Benning, C., and Farré, E.M. (2020). A high-

capacity gene stacking toolkit for the oleaginous microalga, *Nannochloropsis oceanica* CCMP1779. Algal Res. **45:** 101664.

Poliner, E., Pulman, J.A., Zienkiewicz, K., Childs, K., Benning, C., and Farré, E.M. (2018a). A toolkit for *Nannochloropsis oceanica* CCMP1779 enables gene stacking and genetic engineering of the eicosapentaenoic acid pathway for enhanced long-chain polyunsaturated fatty acid production. Plant Biotechnol. J. **16:** 298–309.

Poliner, E., Takeuchi, T., Du, Z.-Y., Benning, C., and Farré, E.M. (2018b). Nontransgenic marker-free gene disruption by an episomal CRISPR system in the oleaginous microalga, *Nannochloropsis oceanica* CCMP1779. ACS Synth. Biol. **7:** 962–968.

Regmi, A., Shockey, J., Kotapati, H.K., and Bates, P.D. (2020). Oil-Producing metabolons containing DGAT1 use separate substrate pools from those containing DGAT2 or PDAT. Plant Physiol. **184:** 720–737.

Reiser, S., and Somerville, C. (1997). Isolation of mutants of *Acinetobacter calcoaceticus* deficient in wax ester synthesis and complementation of one mutation with a gene encoding a fatty acyl-coenzyme A reductase. J. Bacteriol. **179:** 2969–2975.

Ronquist, F., Teslenko, M., van der Mark, P., Ayres, D.L., Darling, A., Höhna, S., Larget, B., Liu, L., Suchard, M.A., and Huelsenbeck, J.P. (2012). MrBayes 3.2: efficient bayesian phylogenetic inference and model choice across a large model space. Syst. Biol. **61:** 539–542.

Sandager, L., Gustavsson, M.H., Ståhl, U., Dahlqvist, A., Wiberg, E., Banaś, A., Lenman, M., Ronne, H., and Stymne, S. (2002). Storage lipid synthesis is non-essential in yeast. J. Biol. Chem. **277:** 6478–6482.

Siaut, M., Heijde, M., Mangogna, M., Montsant, A., Coesel, S., Allen, A., Manfredonia, A., Falciatore, A., and Bowler, C. (2007). Molecular toolbox for studying diatom biology in *Phaeodactylum tricornutum*. Gene **406:** 23–35.

Sorger, D., and Daum, G. (2003). Triacylglycerol biosynthesis in yeast. Appl. Microbiol. Biot. **61**: 289–299.

Ståhl, U., Carlsson, A.S., Lenman, M., Dahlqvist, A., Huang, B., Banaś, W., Banaś, A., and Stymne, S. (2004). Cloning and functional characterization of a phospholipid:diacylglycerol acyltransferase from *Arabidopsis*. Plant Physiol. **135:** 1324–1335.

Vance, J.E. (2015). Phospholipid synthesis and transport in mammalian cells. Traffic **16:** 1–18.

Vieler, A., Brubaker, S.B., Vick, B., and Benning, C. (2012a). A lipid droplet protein of *Nannochloropsis* with functions partially analogous to plant oleosins. Plant Physiol. **158:** 1562–1569.

Vieler, A., Wu, G., Tsai, C.H., Bullard, B., Cornish, A.J., Harvey, C., Reca, I.B., Thornburg, C., Achawanantakun, R., Buehl, C.J., Campbell, M.S., Cavalier, D., Childs, K.L., Clark, T.J., Deshpande, R., Erickson, E., Ferguson, A.A., Handee, W., Kong, Q., Li, X., Liu, B., Lundback, S., Peng, C., Roston, R.L., Sanjaya, Simpson, J.P., TerBush, A., Warakanont, J., Zäuner, S., Farre, E.M., Hegg, E.L., Jiang, N., Kuo, M.H., Lu, Y., Niyogi, K.K., Ohlrogge, J., Osteryoung, K.W., Shachar-Hill, Y., Sears, B.B., Sun, Y., Takahashi, H., Yandell, M., Shiu, S.H., and Benning, C. (2012b). Genome, functional gene annotation, and nuclear transformation of the heterokont oleaginous alga *Nannochloropsis oceanica* CCMP1779. PLoS Genet. **8:** e1003064.

Wang, D., Ning, K, Li, J., Hu, J., Han, D., Wang, H., Zeng, X., Jing, X., Zhou, Q., Su, X., Chang, X., Wang, A., Wang, W., Jia, J., Wei, L., Xin, Y., Qiao, Y., Huang, R., Chen, J., Han, B., Yoon, K., Hill, R.T., Zohar, Y., Chen, F., Hu, Q., and Xu, J. (2014). *Nannochloropsis* genomes reveal evolution of microalgal oleaginous traits. PLoS Genet. **10:** e1004094.

Wang, Q., Lu, Y., Xin, Y., Wei, L., Huang, S., and Xu, J. (2016). Genome editing of model oleaginous microalgae *Nannochloropsis* spp. by CRISPR/Cas9. Plant J. **88:** 1071–1081.

Wang, S., Li, L., Li, H., Sahu, S.K., Wang, H., Xu, Y., Xian, W., Song, B., Liang, H., Cheng, S., Chang, Y., Song, Y., Çebi, Z., Wittek, S., Reder, T., Peterson, M., Yang, H., Wang, J., Melkonian, B., Van de Peer, Y., Xu, X., Wong, G.K.-S., Melkonian, M., Liu, H., and Liu, X. (2020). Genomes of early-diverging streptophyte algae shed light on plant terrestrialization. Nat. Plants **6:** 95–106.

Wang, X., Wei, H., Mao, X., and Liu, J. (2019). Proteomics analysis of lipid droplets from the oleaginous alga *Chromochloris zofingiensis* reveals novel proteins for lipid metabolism. Genom. Proteom. Bioinf. **17:** 260–272.

Wang, Z.T., Ullrich, N., Joo, S., Waffenschmidt, S., and Goodenough, U. (2009). Algal lipid bodies: Stress induction, purification, and biochemical characterization in wild-type and starchless *Chlamydomonas reinhardtii*. Eukaryot. Cell **8:** 1856–1868.

Wei, F., Wang, X., Ma, H., Lv, X., Dong, X., and Chen, H. (2018). Rapid profiling and quantification of phospholipid molecular species in human plasma based on chemical derivatization coupled with electrospray ionization tandem mass spectrometry. Anal. Chim. Acta **1024:** 101e111.

Wei, H., Shi, Y., Ma, X., Pan, Y., Hu, H., Li, Y., Luo, M., Gerken, H., and Liu, J. (2017a). A type-I diacylglycerol acyltransferase modulates triacylglycerol biosynthesis and fatty acid composition in the oleaginous microalga, *Nannochloropsis oceanica*. Biotechnol. Biofuels **10:** 174.

Wei, L., Xin, Y., Wang, Q., Yang, J., Hu, H., and Xu, J. (2017b). RNAi-based targeted gene-knockdown in the model oleaginous microalgae *Nannochloropsis oceanica*. Plant J. **89:** 1236–1250.

Xin, Y., Lu, Y., Lee, Y.-Y., Wei, L., Jia, J., Wang, Q., Wang, D., Bai, F., Hu, H., Hu,

Q., Liu, J., Li, Y., and Xu, J. (2017). Producing designer oils in industrial microalgae by rational modulation of co-evolving type-2 diacylglycerol acyltransferases. Mol. Plant **10:** 1523–1539.

Xin, Y., Shen, C., She, Y., Chen, H., Wang, C., Wei, L., Yoon, K., Han, D., Hu, Q., and Xu, J. (2019). Biosynthesis of triacylglycerol molecules with a tailored PUFA profile in industrial microalgae. Mol. Plant **12:** 474–488.

Xu, Y., Caldo, K. M. P., Pal-Nath, D., Ozga, J., Lemieux, M. J., Weselake, R. J., and Chen, G. (2018). Properties and biotechnological applications of acyl-coa:diacylglycerol acyltransferase and phospholipid:diacylglycerol acyltransferase from terrestrial plants and microalgae. Lipids **53:** 663–688.

Xu, Y., Caldo, K.M.P., Jayawardhane, K., Ozga, J.A., Weselake, R.J., and Chen, G. (2019a). A transferase interactome that may facilitate channeling of polyunsaturated fatty acid moieties from phosphatidylcholine to triacylglycerol. J. Biol. Chem. **294:** 14838-14844.

Xu, Y., Falarz, L., and Chen, G. (2019b). Characterization of type-2 diacylglycerol acyltransferases in the green microalga *Chromochloris zofingiensis*. J. Agr. Food Chem. **67:** 291-298.

Yoon, H.S., Hackett, J.D., Pinto, G., and Bhattacharya, D. (2002). The single, ancient origin of chromist plastids. Proc. Natl. Acad. Sci. U.S.A. **99:** 15507.

Yoon, K., Han, D., Li, Y., Sommerfeld, M. and Hu, Q. (2012). Phospholipid:diacylglycerol acyltransferase is a multifunctional enzyme involved in membrane lipid turnover and degradation while synthesizing triacylglycerol in the unicellular green microalga *Chlamydomonas reinhardtii*. Plant Cell **24:** 3708–3724.

Zhang, C., and Hu, H. (2014). High-efficiency nuclear transformation of the diatom *Phaeodactylum tricornutum* by electroporation. Mar. Genomics **16:** 63–66.

Zhang, M., Fan, J., Taylor, D. C., and Ohlrogge, J. B. (2009). DGAT1 and PDAT1

acyltransferases have overlapping functions in *Arabidopsis* triacylglycerol biosynthesis and are essential for normal pollen and seed development. Plant Cell **21:** 3885–3901.

Zienkiewicz, K., Zienkiewicz, A., Poliner, E., Du, Z.-Y., Vollheyde, K., Herrfurth, C., Marmon, S., Farré, E. M., Feussner, I., and Benning, C. (2017). *Nannochloropsis*, a rich source of diacylglycerol acyltransferases for engineering of triacylglycerol content in different hosts. Biotechnol. Biofuels **10:** 8.

Zienkiewicz, A., Zienkiewicz, K., Poliner, E., Pulman, J.A., Du, Z.-Y., Stefano, G., Tsai, C.-H., Horn, P., Feussner, I., Farre, E.M., Childs, K.L., Brandizzi, F., and Benning, C. (2002). The microalga *Nannochloropsis* during transition from quiescence to autotrophy in response to nitrogen availability. Plant Physiol. **182:** 819-839.

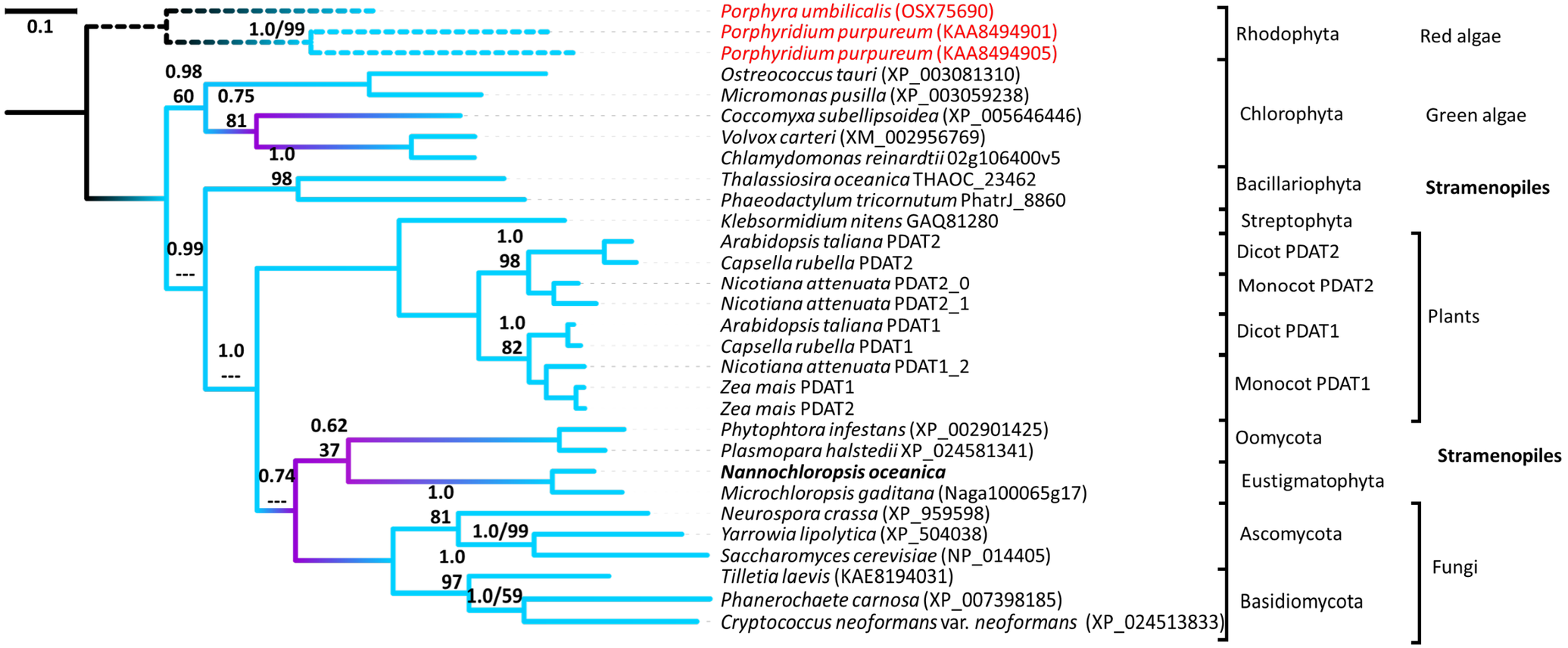

Figure 1. Bayesian and Maximum Likelihood (ML) phylogenetic analyses of PDATs from different phyla. The Basien tree only is represented here and is drawn to scale, with branch lengths measured in the number of substitutions per site. The posterior probability (PP) from the Bayesian analysis and the bootstrap value from the ML analysis are reported on the nodes. The nodes where PP equals 1.0 and ML support equals 100 were removed. --- = node not present in ML. Rhodophyte sequences (red) were used as outgroup to root both Bayesian and ML trees.

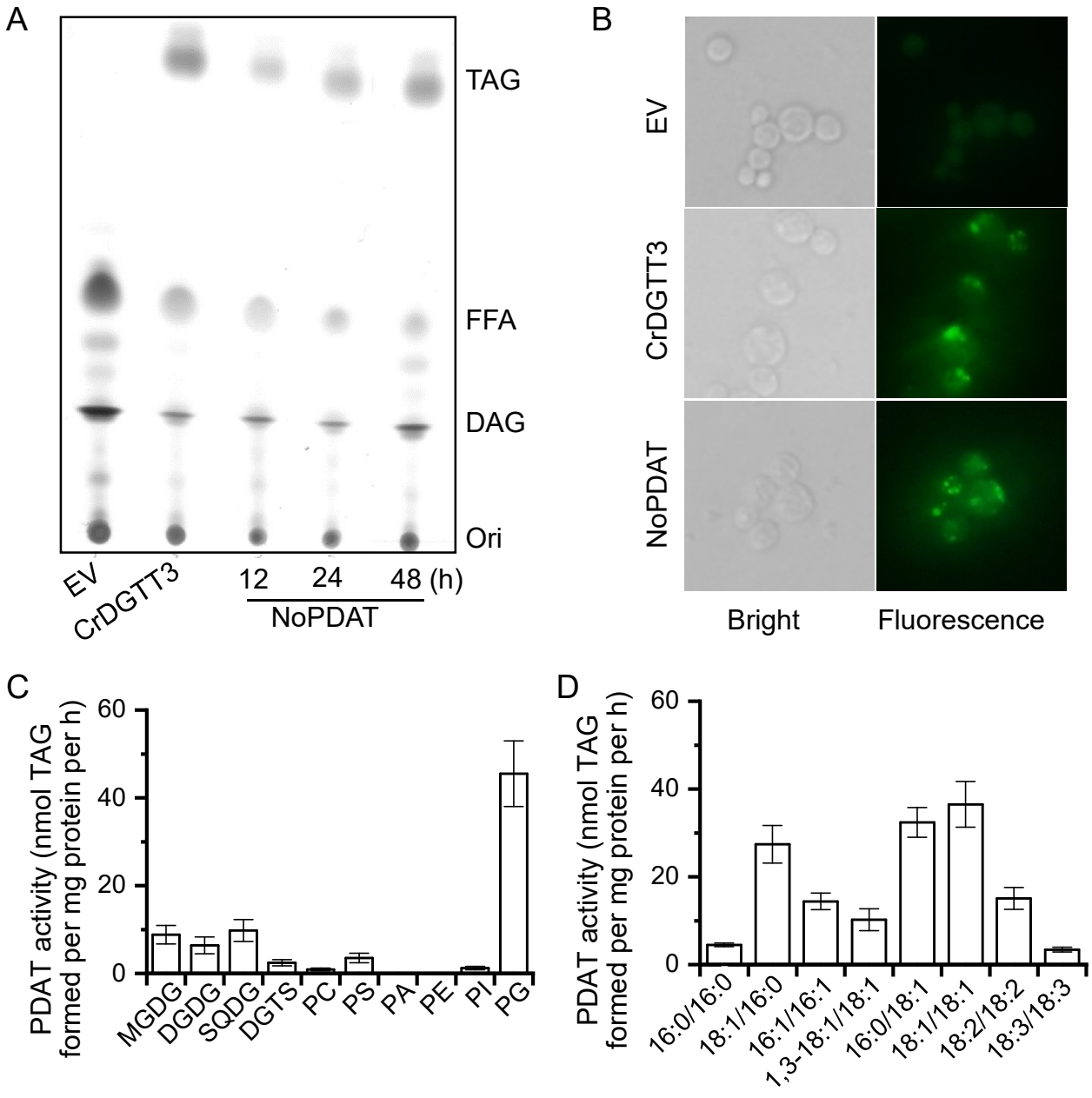

Figure 2. Characterization of NoPDAT activity. (A, B) Functional complementation of NoPDAT in TAG-deficient *S. cerevisiae* H1246 cells as determined by TLC analysis of lipid extracts (A) and Bodipy staining (B) of NoPDAT-expressing H1246 cells. EV (empty vector) and CrDGTT3 (Liu et al., 2016) were used as negative and positive controls, respectively. (C, D) Substrate preference of NoPDAT for polar lipids (C) and DAGs (D). DAG (18:1/18:1) was used as the acyl acceptor in (C) and PG was used as the acyl donor in (D). Data represent mean ± SD (n=3).

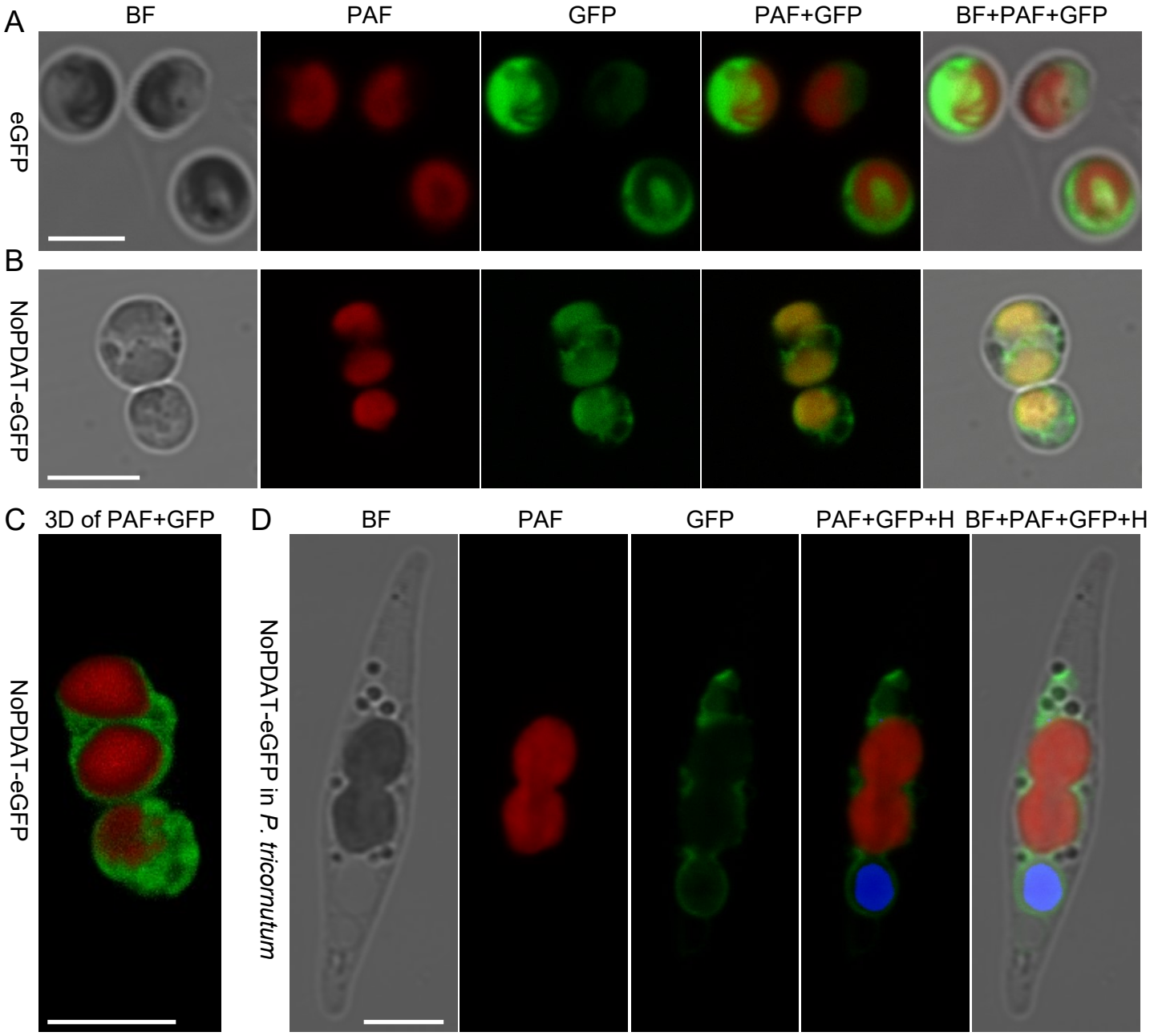

Figure 3. Subcellular localization of NoPDAT in *N. oceanica* and *P. tricornutum* cells. (A, B) *N. oceanica* cells transformed with the empty vector (eGFP, A) and NoPDAT-eGFP (B). (C) A 3D visualization of PAF+GFP in (B). (D) *P. tricornutum* cells transformed with NoPDAT-eGFP. BF, bright field; PAF, plastid autofluorescence; H, Hoechst. Red indicates the plastid autofluorescence (PAF), green indicates the GFP signal, while blue indicates the staining of nucleus with Hoechst (H). Bar, 4 μm.

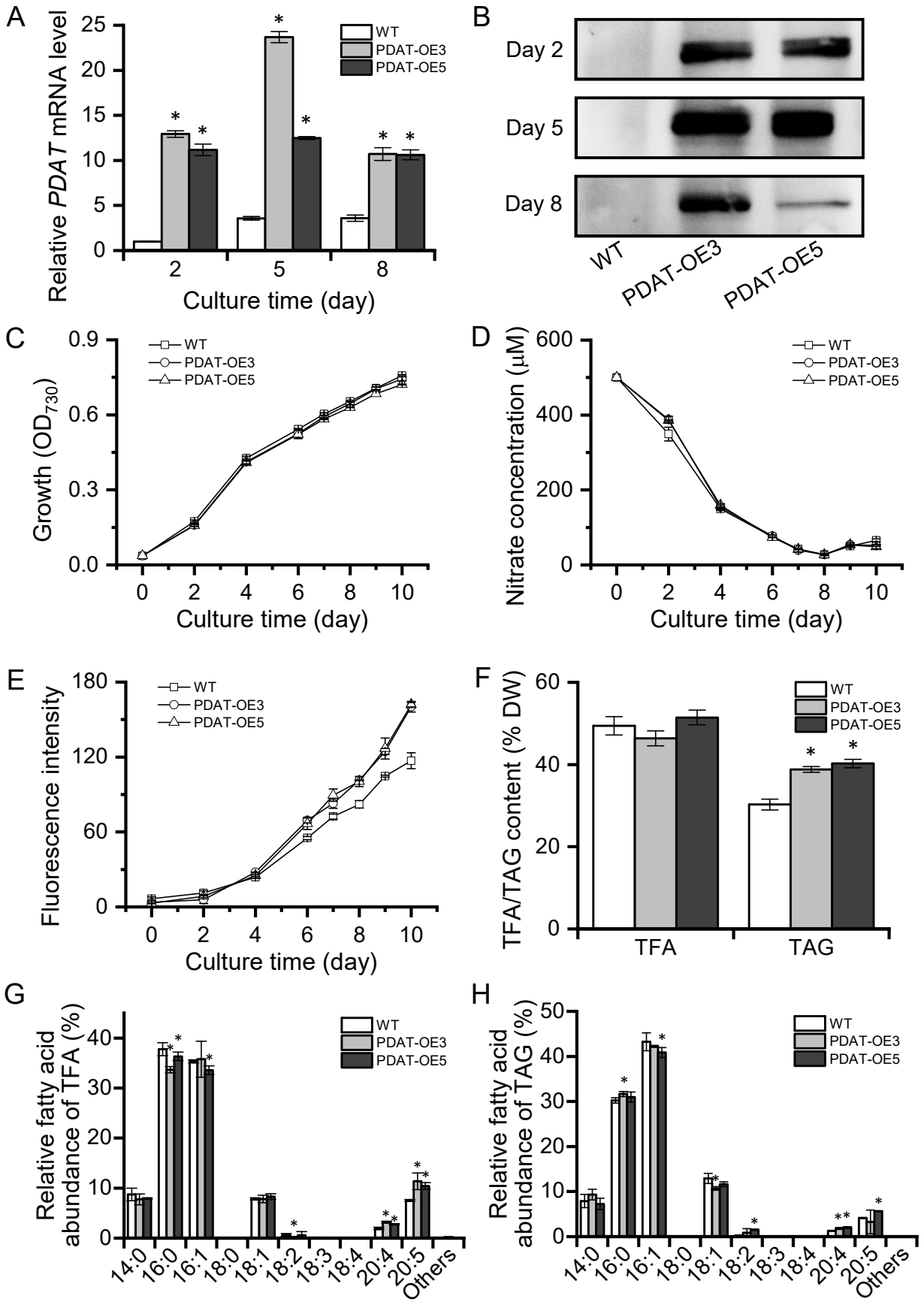
A
Relative PDAT mRNA level
25
20
15
10
5
0
2
5
8
Culture time (day)
WT
PDAT-OE3
PDAT-OE5
B
Day 2
Day 5
Day 8
WT
PDAT-OE3
PDAT-OE5
C
Growth (OD730)
0.9
0.6
0.3
0.0
0
2
4
6
8
10
Culture time (day)
WT
PDAT-OE3
PDAT-OE5
D
Nitrate concentration (μM)
600
400
200
0
0
2
4
6
8
10
Culture time (day)
WT
PDAT-OE3
PDAT-OE5
E
Fluorescence intensity
180
120
60
0
0
2
4
6
8
10
Culture time (day)
WT
PDAT-OE3
PDAT-OE5
F
TFA/TAG content (% DW)
60
40
20
0
TFA
TAG
WT
PDAT-OE3
PDAT-OE5
G
Relative fatty acid abundance of TFA (%)
40
30
20
10
0
14:0
16:0
16:1
18:0
18:1
18:2
18:3
18:4
20:4
20:5
Others
WT
PDAT-OE3
PDAT-OE5
H
Relative fatty acid abundance of TAG (%)
50
40
30
20
10
0
14:0
16:0
16:1
18:0
18:1
18:2
18:3
18:4
20:4
20:5
Others
WT
PDAT-OE3
PDAT-OE5

Figure 4. Characterization of *NoPDAT* overexpression lines of *N. oceanica*. (A) *NoPDAT* mRNA level in wild-type (WT) and the two *NoPDAT* overexpression lines (PDAT-OE3 and PDAT-OE5), as determined by qPCR. The *NoPDAT* expression in WT on day 2 was used as the reference (set as 1). (B) NoPDAT protein level in in WT and the two *NoPDAT* overexpression lines, as determined by immunoblotting. (C) Growth curve as determined by OD_{730}. (D) Nitrate concentration in the culture medium. (E) Fluorescence intensity of Nile Red-stained algal cells. (F) Content of total fatty acid (TFA) and TAG from the 8-day cultures. (G, H) Relative fatty acid abundance of TFA (G) and TAG (H) from the 8-day cultures. Data in (A and C-H) represent mean ± SD (n=3). * indicates statistically significant differences from WT values at $P < 0.05$ level.

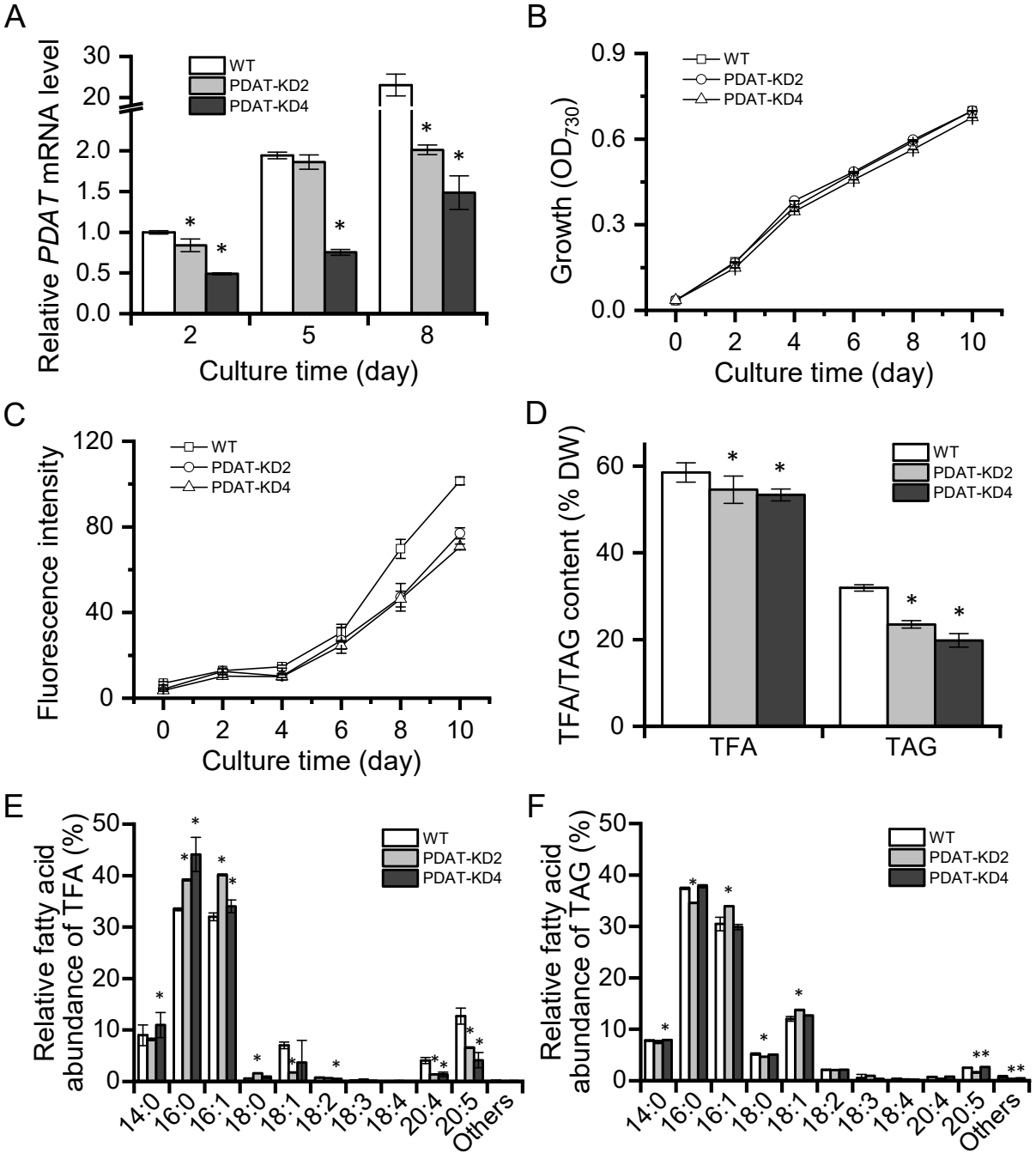

Figure 5. Characterization of *NoPDAT* knockdown lines of *N. oceanica*. (A) *NoPDAT* mRNA level in wild-type (WT) and the two *NoPDAT* knockdown lines (PDAT-KD2 and PDAT-KD4), as determined by qPCR. The *NoPDAT* expression in WT on day 2 was used as the reference (set as 1). (B) Growth curve as determined by OD_{730}. (C) Fluorescence intensity of Nile Red-stained algal cells. (D) Content of total fatty acid (TFA) and TAG from the 8-day cultures. (E, F) Relative fatty acid abundance of TFA (E) and TAG (F) from the 8-day cultures. Data represent mean ± SD (n=3). * indicates statistically significant differences from WT values at $P < 0.05$ level.

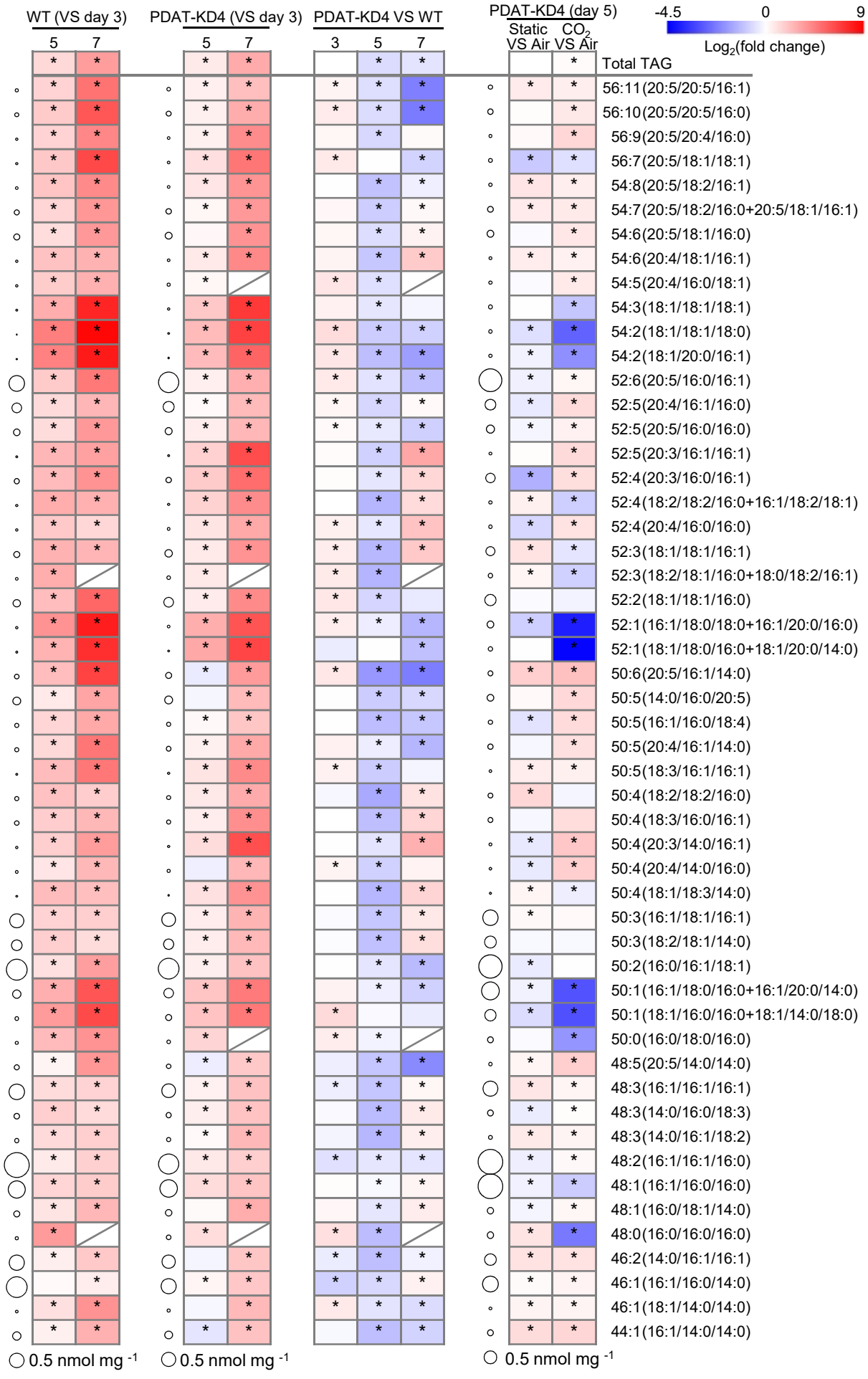
WT (VS day 3)
5
7
PDAT-KD4 (VS day 3)
5
7
PDAT-KD4 VS WT
3
5
7
PDAT-KD4 (day 5)
Static VS Air
CO2 VS Air
-4.5
0
9
Log2(fold change)
Total TAG
56:11(20:5/20:5/16:1)
56:10(20:5/20:5/16:0)
56:9(20:5/20:4/16:0)
56:7(20:5/18:1/18:1)
54:8(20:5/18:2/16:1)
54:7(20:5/18:2/16:0+20:5/18:1/16:1)
54:6(20:5/18:1/16:0)
54:6(20:4/18:1/16:1)
54:5(20:4/16:0/18:1)
54:3(18:1/18:1/18:1)
54:2(18:1/18:1/18:0)
54:2(18:1/20:0/16:1)
52:6(20:5/16:0/16:1)
52:5(20:4/16:1/16:0)
52:5(20:5/16:0/16:0)
52:5(20:3/16:1/16:1)
52:4(20:3/16:0/16:1)
52:4(18:2/18:2/16:0+16:1/18:2/18:1)
52:4(20:4/16:0/16:0)
52:3(18:1/18:1/16:1)
52:3(18:2/18:1/16:0+18:0/18:2/16:1)
52:2(18:1/18:1/16:0)
52:1(16:1/18:0/18:0+16:1/20:0/16:0)
52:1(18:1/18:0/16:0+18:1/20:0/14:0)
50:6(20:5/16:1/14:0)
50:5(14:0/16:0/20:5)
50:5(16:1/16:0/18:4)
50:5(20:4/16:1/14:0)
50:5(18:3/16:1/16:1)
50:4(18:2/18:2/16:0)
50:4(18:3/16:0/16:1)
50:4(20:3/14:0/16:1)
50:4(20:4/14:0/16:0)
50:4(18:1/18:3/14:0)
50:3(16:1/18:1/16:1)
50:3(18:2/18:1/14:0)
50:2(16:0/16:1/18:1)
50:1(16:1/18:0/16:0+16:1/20:0/14:0)
50:1(18:1/16:0/16:0+18:1/14:0/18:0)
50:0(16:0/18:0/16:0)
48:5(20:5/14:0/14:0)
48:3(16:1/16:1/16:1)
48:3(14:0/16:0/18:3)
48:3(14:0/16:1/18:2)
48:2(16:1/16:1/16:0)
48:1(16:1/16:0/16:0)
48:1(16:0/18:1/14:0)
48:0(16:0/16:0/16:0)
46:2(14:0/16:1/16:1)
46:1(16:1/16:0/14:0)
46:1(18:1/14:0/14:0)
44:1(16:1/14:0/14:0)
0.5 nmol mg -1
0.5 nmol mg -1
0.5 nmol mg -1

Figure 6. Heat map illustrating the variation of TAG species. The data are expressed as $\log_2$(fold change) values (n=3) for wild-type (WT) (day 5 and 7, VS day 3), *NoPDAT* knockdown line (PDAT-KD4) (day 5 and 7, VS day 3), PDAT-KD4 VS WT (day 3, 5 and 7), and PDAT-KD4 on day 5 (static VS Air and CO_2 VS Air). The circle at the left of the heat map designate the content of individual TAG species for WT on day 3 (1st circle column), PDAT-KD4 on day 3 (2nd circle column), and PDAT-KD4 on day 5 (3rd circle column). Static, static culture; Air, culture aerated with air; CO_2, culture aerated with 2% CO_2. Significant difference (Student's *t*-test, $P < 0.01$) is indicated with an asterisk.

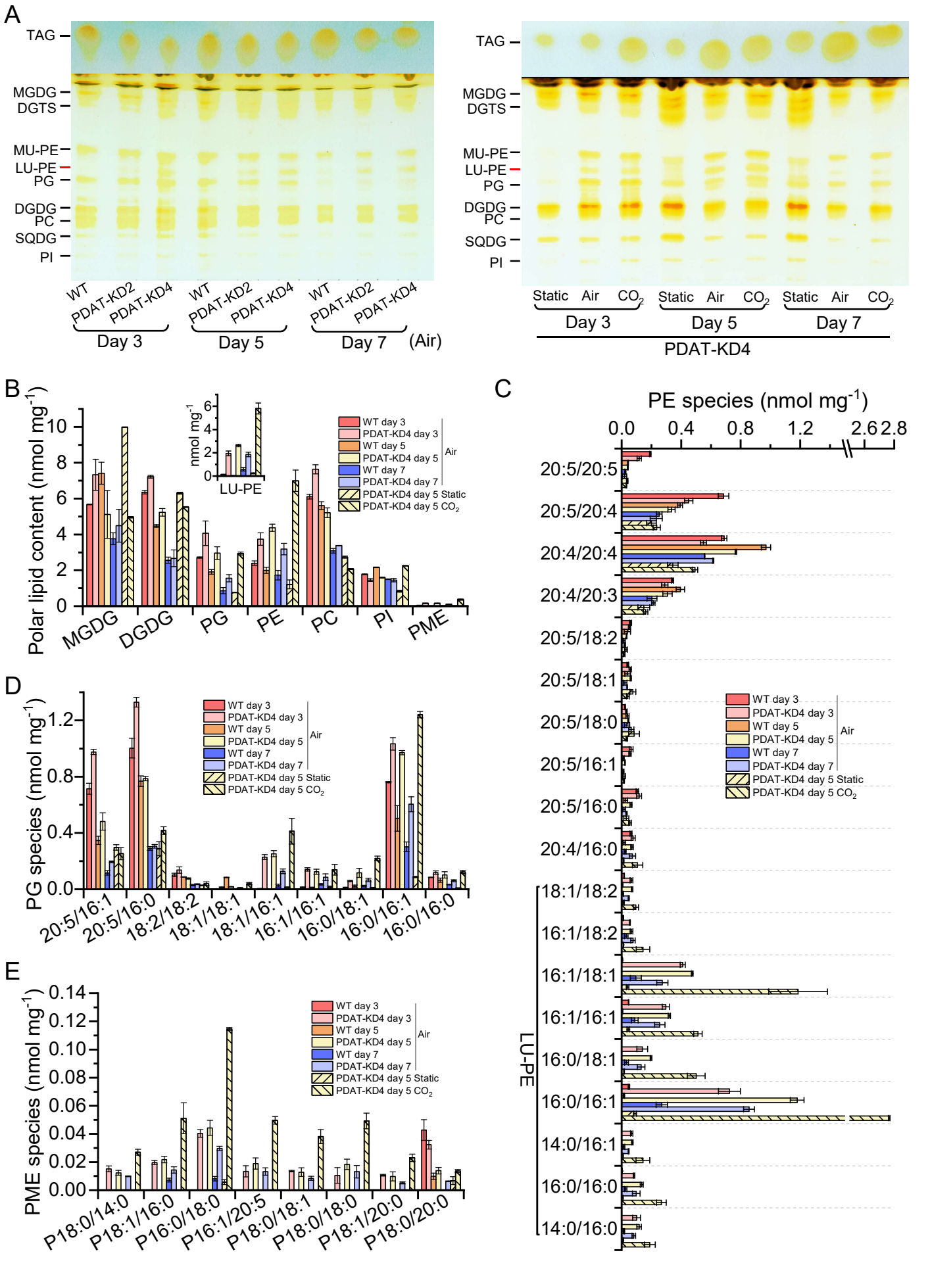
A
TAG
MGDG
DGTS
MU-PE
LU-PE
PG
DGDG
PC
SQDG
PI
WT
PDAT-KD2
PDAT-KD4
Day 3
Day 5
Day 7
(Air)
Static
Air
CO2
PDAT-KD4
B
Polar lipid content (nmol mg-1)
MGDG
DGDG
PG
PE
PC
PI
PME
nmol mg-1
LU-PE
WT day 3
PDAT-KD4 day 3
WT day 5
PDAT-KD4 day 5
WT day 7
PDAT-KD4 day 7
PDAT-KD4 day 5 Static
PDAT-KD4 day 5 CO2
Air
C
PE species (nmol mg-1)
20:5/20:5
20:5/20:4
20:4/20:4
20:4/20:3
20:5/18:2
20:5/18:1
20:5/18:0
20:5/16:1
20:5/16:0
20:4/16:0
18:1/18:2
16:1/18:2
16:1/18:1
16:1/16:1
16:0/18:1
16:0/16:1
14:0/16:1
16:0/16:0
14:0/16:0
LU-PE
D
PG species (nmol mg-1)
20:5/16:1
20:5/16:0
18:2/18:2
18:1/18:1
18:1/16:1
16:1/16:1
16:0/18:1
16:0/16:1
16:0/16:0
E
PME species (nmol mg-1)
P18:0/14:0
P18:1/16:0
P16:0/18:0
P16:1/20:5
P18:0/18:1
P18:0/18:0
P18:1/20:0
P18:0/20:0

Figure 7. Effect of *NoPDAT* knockdown on polar lipids of *N. oceanica*. (A) TLC analysis of lipid extracts from wild-type (WT) and *NoPDAT* knockdown lines (PDAT-KD2 and PDAT-KD4) aerated with air (left) and PDAT-KD4 under different CO_2 availability conditions (right). (B) Content of polar lipids. (C-E) Content of PE species (C), PG species (D) and PME species (E). Static, static culture; Air, culture aerated with air; CO_2, culture aerated with 2% CO_2. Data represent mean ± SD (n=3). MU-PE: "more-unsaturated PE", PE enriched in 20:3, 20:4 and 20:5 fatty acids; LU-PE: "less-unsaturated PE", PE enriched in saturated or monounsaturated fatty acids; PME: plasmenylethanolamine.

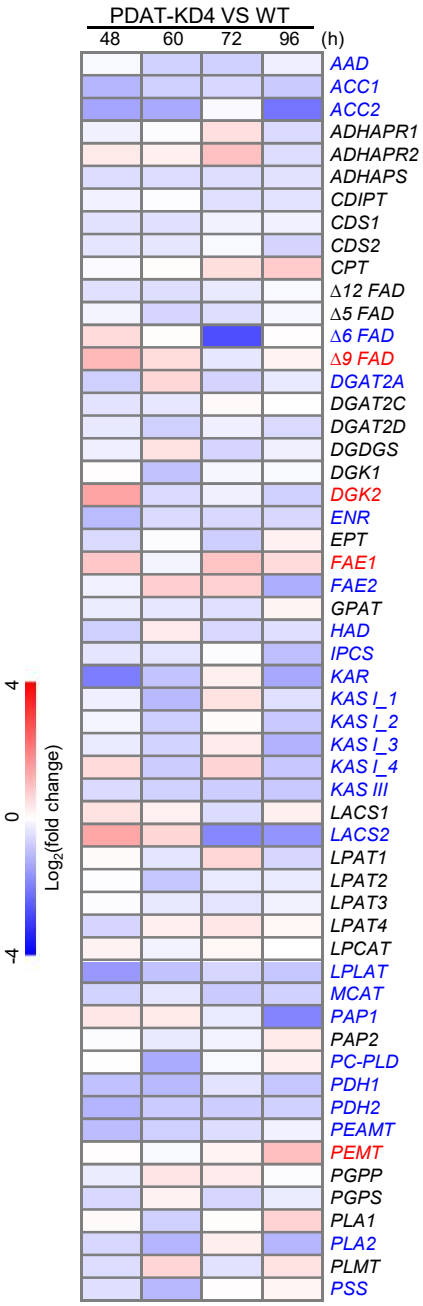

Figure 8. The effect of *NoPDAT* knockdown on lipid metabolism network in *N. oceanica*. Four time points were selected for qPCR. Genes were considered to be significantly differentially expressed if: the expression level fold change between *NoPDAT* knockdown line (PDAT-KD4) and wild-type (WT) was no less than 2-fold with $P < 0.01$ for at least one time point or no less than 1.5-fold with $P < 0.01$ for at least two time points. The genes in blue and red were down- and up-regulated, respectively. Abbreviations: AAD (acyl-ACP desaturase); ACC (acetyl-CoA carboxylase); ADHAPR (acyl/alkyl-dihydroxyacetone phosphate reductase); ADHAPS (alkyl-dihydroxyacetone phosphate synthase); CDIPT (CDP-diacylglycerol-inositol 3-phosphatidyltransferase); CDS (CDP-diacylglycerol synthase); CPT (choline phosphotransferase); Δ12 FAD (Δ12-fatty acid desaturase); Δ5 FAD (Δ5-fatty acid desaturase); Δ6 FAD (Δ6-fatty acid desaturase); Δ9 FAD (stearoyl-CoA 9-desaturase); DGAT (diacylglycerol acyltransferase); DGDGS (digalactosyldiacylglycerol synthase); DGK (diacylglycerol kinase); ENR (enoyl-ACP reductase); EPT (ethanolamine phosphotransferase); FAE (fatty acid elongase); GPAT (glycerol-3-phosphate acyltransferase); HAD (hydroxyacyl-ACP dehydrase); IPCS (inositol phosphorylceramide synthase); KAR (ketoacyl-ACP reductase); KAS (ketoacyl-ACP synthase); LACS (long-chain acyl-CoA synthetase); LPAT (lysophosphatidic acid acyltransferases); LPCAT (lysophosphatidylcholine acyltransferase); LPLAT (lysophospholipid acyltransferase); MCAT (malonyl-CoA:ACP transacylase); PAP (phosphatidic acid phosphatase); PC-PLD (phosphatidylcholine-specific phospholipase D); PDH (pyruvate dehydrogenase); PEAMT (phosphoethanolamine *N*-methyltransferase); PEMT (phosphatidylethanolamine *N*-methyltransferase); PGPP (phosphatidylglycerolphosphate phosphatase); PGPS (phosphatidylglycerolphosphate synthase); PLA (phospholipase A); PLMT (phospholipid *N*-methyltransferase); PSS (phosphatidylserine synthase).

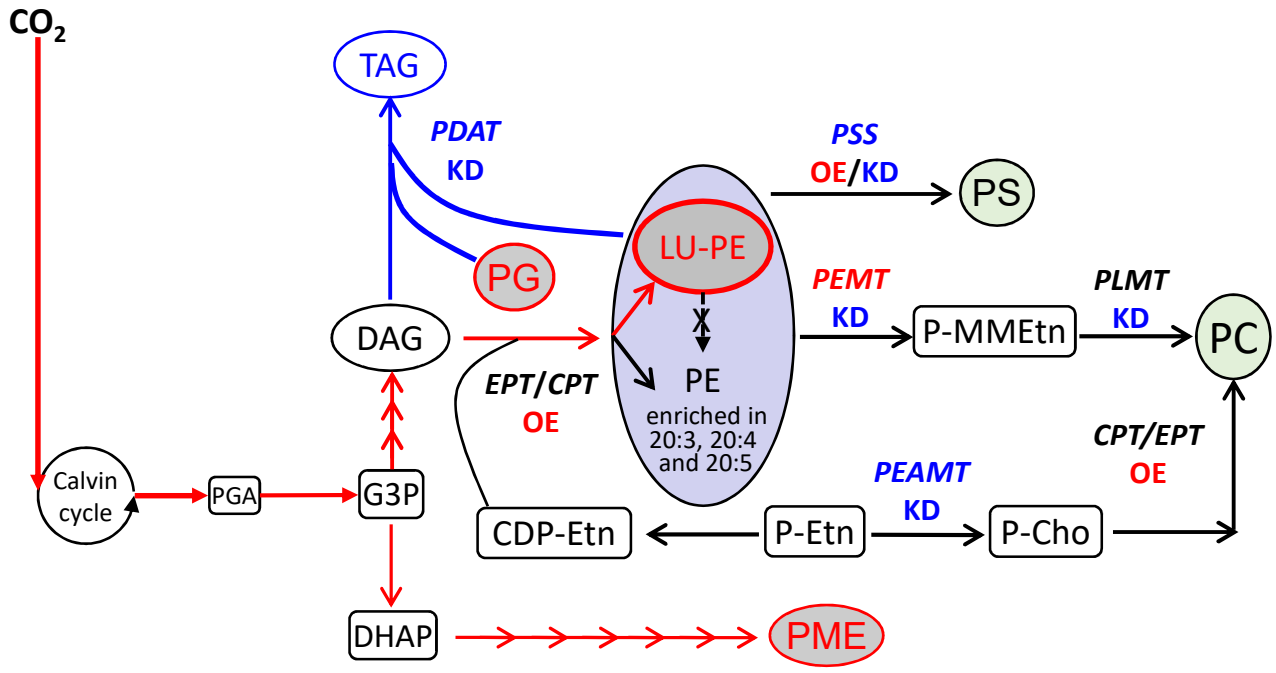

Figure 9. A hypothesized working model illustrating the role of NoPDAT in lipid metabolism in *N. oceanica*. Down-regulated genes and decreased metabolite by *PDAT* knockdown (KD) are illustrated in blue, and up-regulated gene, increased metabolites and carbon flux by *PDAT* KD in red. Knockdown (KD) and overexpression (OE) of genes involved in PE homeostasis that were carried out in the study are also shown in the model. PGA (3-phosphoglyceric acid); G3P (Glycerol 3-phosphate); DHAP (dihydroxyacetone phosphate); CDP-Etn (cytidine diphosphate-ethanolamine); P-Etn (phosphoethanolamine); P-Cho (phosphocholine); P-MMEtn (phospho-monomethyl-ethanolamine);CPT (cholinephosphotranferase); EPT (ethanolaminephosphotranferase); PSS (phosphatidylserine synthase); PEMT (phosphatidylethanolamine N-methyltransferase); PLMT (phospholipid N-methyltransferase); PEAMT (phosphoethanolamine methyltransferase); LU-PE: "less-unsaturated PE", PE enriched in saturated or monounsaturated fatty acids; PME: plasmenylethanolamine.

Supplemental Figure 1. Sequence alignment of the amino acids of phospholipid:diacylglycerol acyltransferase (PDAT). The seven most characteristically conserved domains are shown and predicated transmembrane domain in *Nannochloropsis oceanica* PDAT (NoPDAT) are boxed. AtPDAT1, *Arabidopsis thaliana* PDAT1; AtPDAT2, *A. thaliana* PDAT2; ScPDAT, *Saccharomyces cerevisiae* PDAT; PtPDAT, *Phaeodactylum tricornutum* PDAT; TpPDAT, *Thalassiosira pseudonana* PDAT; NgPDAT, *Nannochloropsis gaditana*. Arrows indicate catalytic triad (Ser-Asp-His).

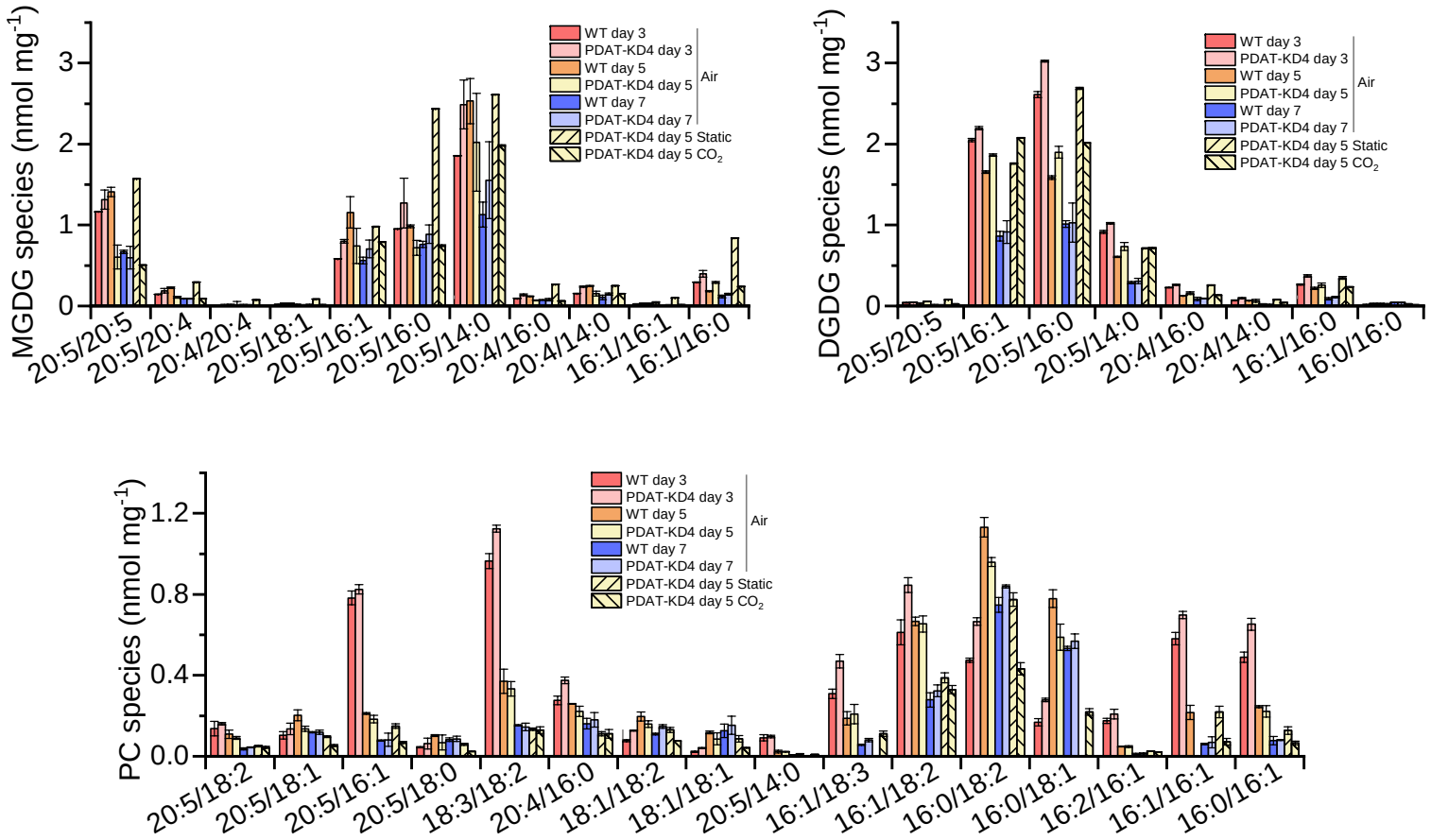

Supplemental Figure 2. Content of MGDG, DGDG and PC species in wild-type (WT) and the *NoPDAT* knockdown line (PDAT-KD4) of *Nannochloropsis oceanica*. Static, static culture; Air, culture aerated with air; CO_2, culture aerated with 2% CO_2. Data represent mean ± SD (*n*=3).

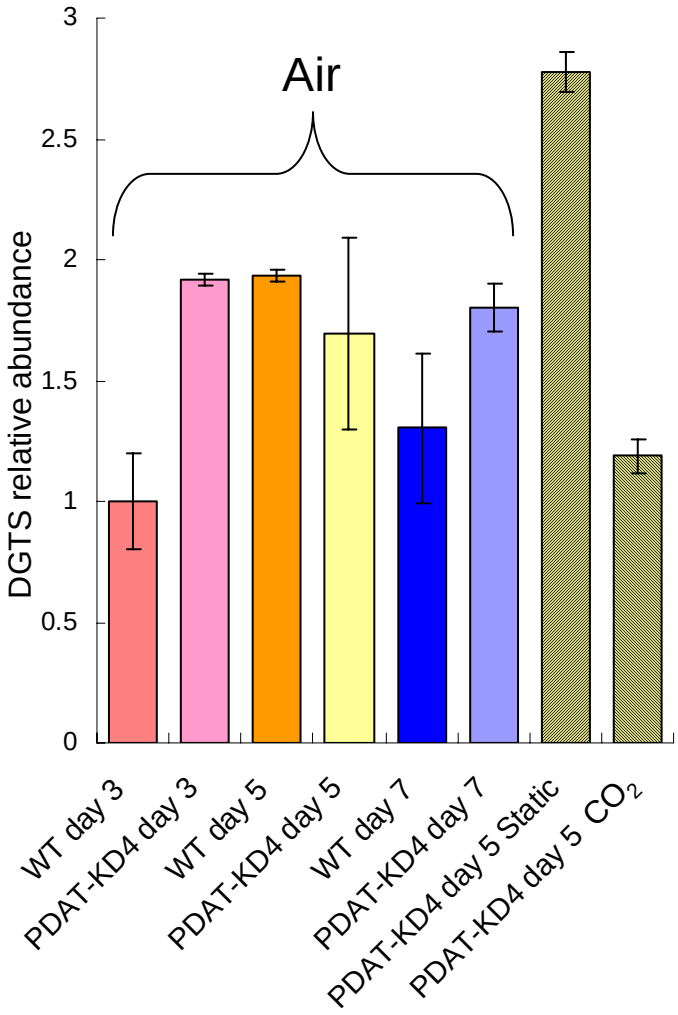

Supplemental Figure 3. Effect of *NoPDAT* knockdown on DGTS of *Nannochloropsis oceanica* as determined by TLC analysis (the abundance of wild-type on day 3 was set as 1). Static, static culture; Air, culture aerated with air; CO_2, culture aerated with 2% CO_2. Data represent mean ± SD (*n*=3). WT, wild-type; PDAT-KD4, *NoPDAT* knockdown line 4.

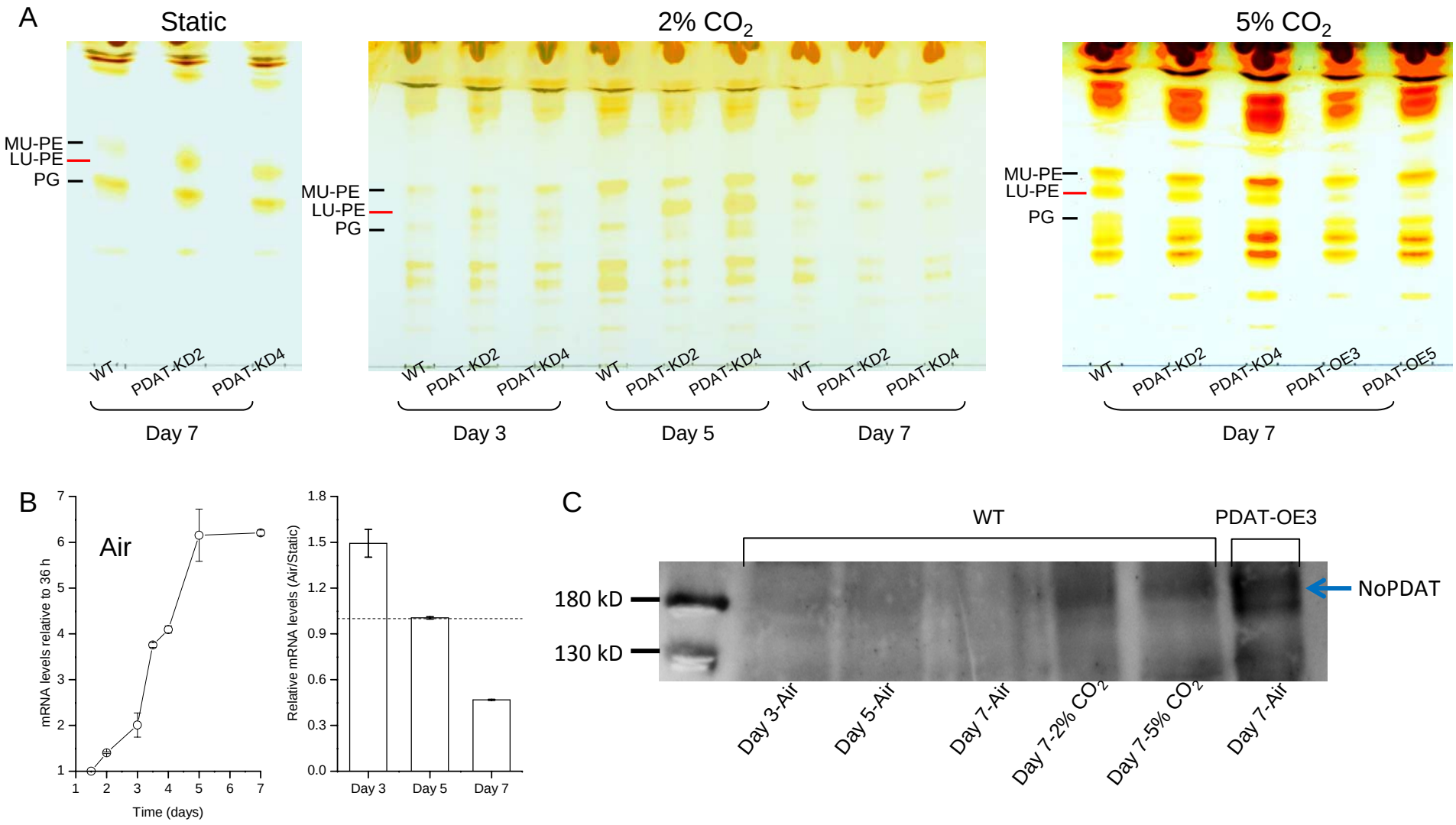

Supplemental Figure 4. Effect of culture conditions on LU-PE accumulation (A), *NoPDAT* mRNA (B, determined by qPCR) and protein (C, determined by immunoblotting) levels in wild-type (WT), *NoPDAT* knockdown (PDAT-KD2 and PDAT-KD4) and overexpression lines (PDAT-OE3 and PDAT-OE5) of *Nannochloropsis oceanica*. Static, static culture; Air, culture aerated with air; 2% CO_2, culture aerated with 2% CO_2; 5% CO_2, culture aerated with 5% CO_2. MU-PE: "more-unsaturated PE", PE enriched in 20:3, 20:4 and 20:5 fatty acids; LU-PE: "less-unsaturated PE", PE enriched in saturated or monounsaturated fatty acids. The *NoPDAT* mRNA levels under air condition at 36 h (B, left) or under static condition (B, right, dot line) was set as 1.

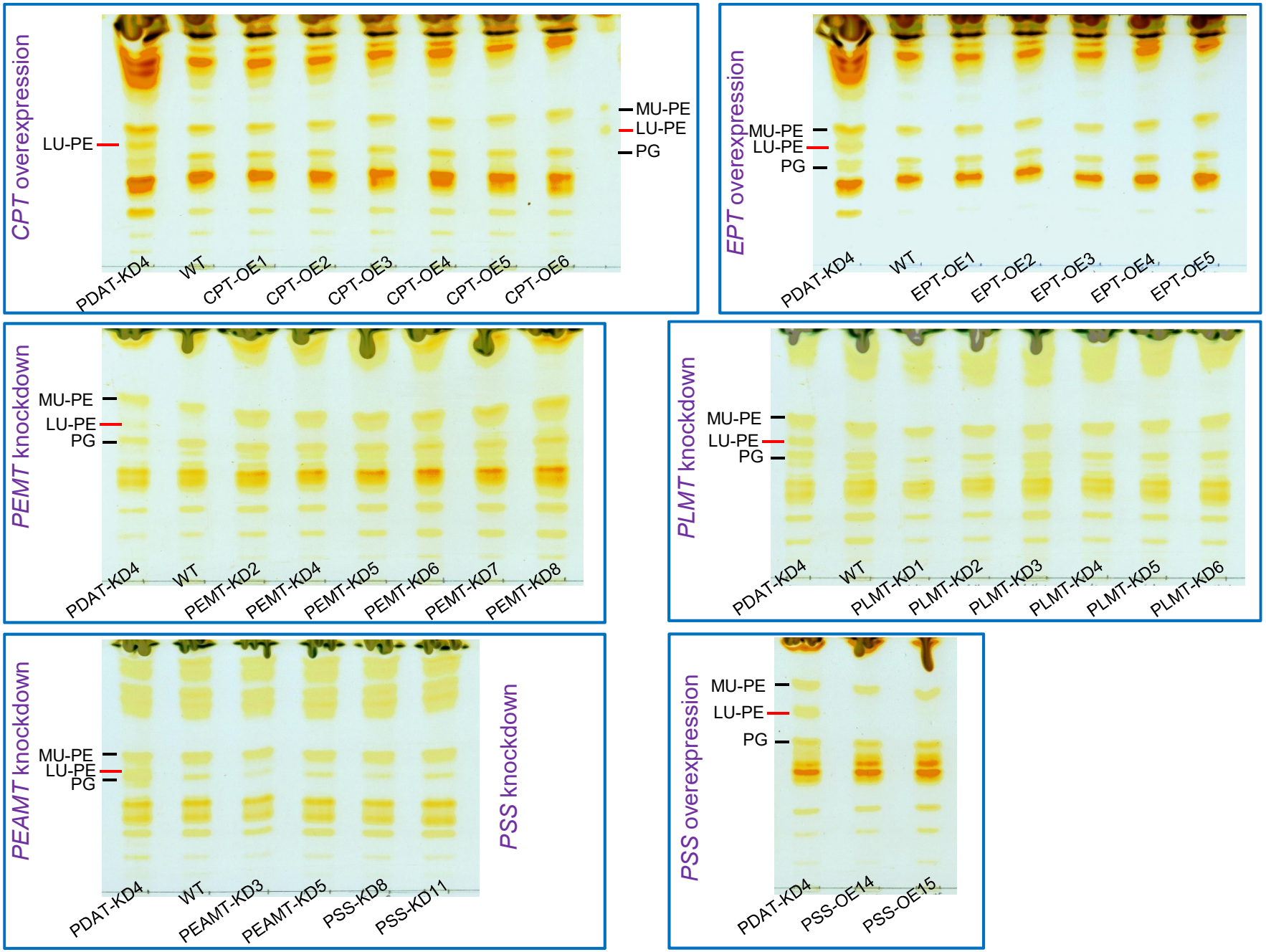

Supplemental Figure 5. Effect of *CPT* overexpression (CPT-OE1~6), *EPT* overexpression (EPT-OE1~5), *PEMT* knockdown (PEMT-KD2, 4~8), *PLMT* knockdown (PLMT-KD1~6), *PEAMT* knockdown (PEAMT-KD3, 5), *PSS* knockdown (PSS-KD8, 11) and *PSS* overexpression (PSS-OE14, 15) on LU-PE accumulation in *N. oceanica*. MU-PE: "more-unsaturated PE", PE enriched in 20:3, 20:4 and 20:5 fatty acids; LU-PE: "less-unsaturated PE", PE enriched in saturated or monounsaturated fatty acids.

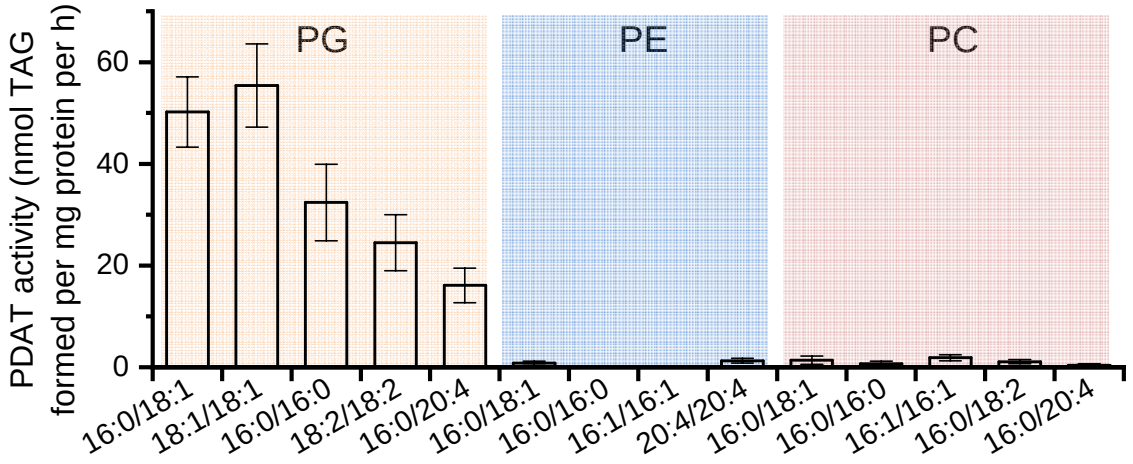

Supplemental Figure 6. *In vitro* assay of NoPDAT on PE, PC and PG with various acyl compositions.

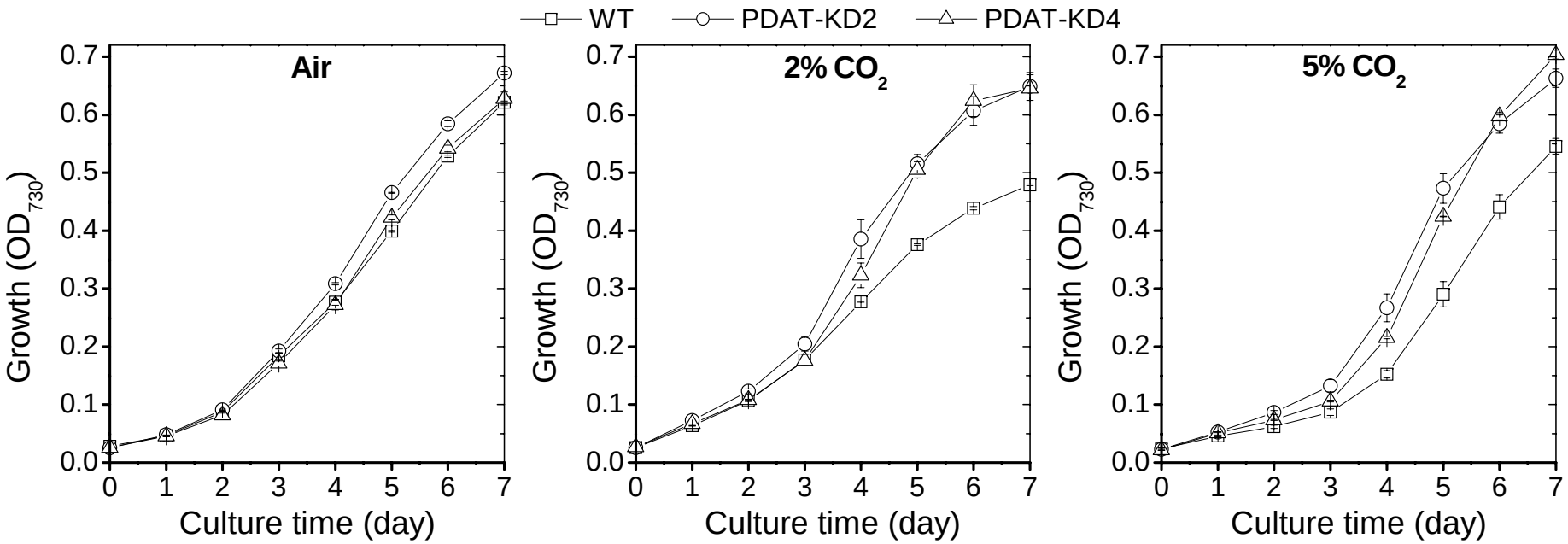

Supplemental Figure 7. Growth curves of wild-type (WT) and *NoPDAT* knockdown lines (PDAT-KD2 and PDAT-KD4) of *Nannochloropsis oceanica* aerated with air, 2% CO_2 or 5% CO_2.

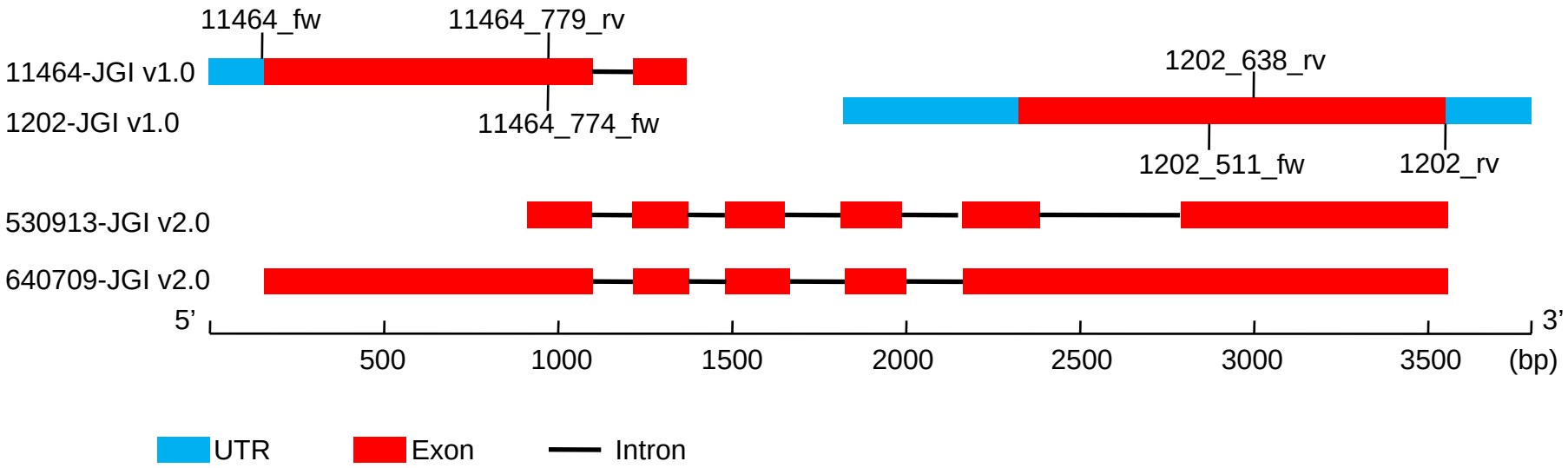

Supplemental Figure 8. Gene structures of the *Nannochloropsis oceanica PDAT* annotated in JGI v1 (11464, 1202) and v2 (530913, 640709).